Composite Structures xxx (2020) 113291

Contents lists available at ScienceDirect

Composite Structures

journal homepage: www.elsevier.com/locate/compstruct

Hybrid UHPC/NSM CFRP strips vs. traditional systems for flexural upgrading of RC beams – Experimental and FE study

Hussein M. Elsanadedy [1,*], Husain Abbas, Tarek H. Almusallam, Yousef A. Al-Salloum

Department of Civil Eng., College of Eng., King Saud University, P.O. Box 800, Riyadh 11421, Saudi Arabia

ARTICLE INFO

Keywords:
RC beams
Flexural strengthening
FRP sheets
NSM
FRCM composites
FE

ABSTRACT

In this study, the efficacy of traditional versus innovative systems for enhancing the flexural strength of RC (reinforced concrete) beams is investigated experimentally as well as numerically. Four-point bending tests were conducted on seven RC beams. Test matrix comprised of two control and five strengthened beams. Strengthening techniques included: bonded steel plate, externally attached CFRP (carbon fiber reinforced polymer) composite, NSM (near-surface mounted) steel rebars, externally attached CFRCM (carbon fiber reinforced cementitious matrix) composite, and innovative hybrid system comprising of ultra-high performance concrete (UHPC) layer combined with NSM CFRP strips. Different strengthening systems were designed to provide approximately the same flexural strength enhancement. The performance of strengthened specimens was compared in terms of load–deflection characteristics. The peak load of the tested specimens was analytically predicted using the equations of ACI 318-19 code and ACI 440.2R-17 guidelines. Nonlinear FE (finite element) modeling was also carried out, and a comparison was conducted between the experimental and FE results showing good agreement. The validated FE models were extended for some useful parametric studies of interest.

1. Introduction

Rehabilitation of RC (reinforced concrete) structures is regularly needed because of: (a) increase in demanded load; (b) damage caused by material aging, corrosion of steel reinforcement, and/or exposure to fire; (c) alterations in the structural system owing to the removal of columns/ load-bearing walls; (d) faults in structural design or construction causing insufficient cross-section dimensions; (e) and/or inadequate steel reinforcement; or (f) the need to comply with the current seismic design codes [1].

As RC beams are critical structural members, they may, if deficient, result in the partial collapse of the structure. Therefore, RC beams may need strengthening in flexure, shear, or both. The most common flexural strengthening systems for RC beams comprise: section enlargement, externally bonded steel plates, planting of NSM (near-surface mounted) steel or fiber reinforced polymer (FRP) rebars, and externally attached FRP or FRCM (fiber reinforced cementitious matrix) composites [2–14]. These strengthening systems are concisely discussed below.

Section enlargement technique requires the placement of formwork around the beam section to increase its size with new concrete and steel rebars. This technique causes enhancement in the stiffness and flexural strength of RC beams. This technique essentially needs a proper treatment of the concrete surface for having the monolithic action between old and new concrete [3]. Even though this technique was found to be an efficient and affordable system, it reduces available clearance and adds extra weight to the beam. Additionally, it is a labor-intensive technique [15].

As a traditional technique, externally bonded steel plates are employed for flexural upgrading of RC beams. This technique was found to be efficient at enhancing the flexural capacity, while minimizing the service-load deflection. The advantages of this technique include reduced cost, less interruption, and no need of skilled labor [4]. Nevertheless, the drawbacks of this system comprise the reduction of available clearance, the proneness of plates to corrosion, and weight increase.

Another flexural strengthening technique for RC beams is the use of NSM rebars. In this technique, steel (or FRP) rebars are laid in grooves that are cut in the surface cover, and these grooves are then filled with

* Corresponding author.
E-mail addresses: helsanadedy@ksu.edu.sa, elsanadedy@yahoo.com (H.M. Elsanadedy).
[1] On leave from Helwan Univ., Cairo, Egypt

https://doi.org/10.1016/j.compstruct.2020.113291
Received 25 April 2020; Revised 26 July 2020; Accepted 1 November 2020
Available online xxxx

epoxy-based (or cementitious) mortar [5]. This system was launched in Europe for NSM steel rebars, but recently with the availability of FRP material, the steel rebars are substituted by FRP rebars [16].

Jung et al. [17] investigated the observed failure modes of 106 RC beams available in the literature and strengthened in flexure using NSM FRP reinforcement. It was revealed that failure of strengthened beams occurred due to: (1) concrete cover delamination in which the original tensile steel rebars acted as a bond breaker, and the concrete cover separates from the rest of the beam (55% of specimens); (2) rupture of FRP reinforcement at the maximum-moment zone (35% of specimens); or (3) bond failure at the filler-to-concrete interface (10% of specimens).

For the past years, FRP materials have been successfully utilized in the flexural upgrading of RC beams [6–8]. This may be owing to the advantages of these materials, for example, superior strength-to-weight ratio, ease and speed of installation, anti-corrosion, insignificant reduction of available clearance, insignificant increase in beam weight, and minimum interruption of services [18]. In spite of these advantages, FRP composites also have some disadvantages, which are associated with the used epoxy resins [19]. These drawbacks comprise: (i) bad performance of epoxy resins at a high temperature exceeding the glass transition temperature; (ii) debonding at FRP/concrete interface; (iii) expensive epoxies; (iv) incapability of applying FRP composites at low temperatures or on wet surfaces; and (v) difficulty in performing post-earthquake damage assessment to substrate concrete behind the FRP sheets. As a possible solution to the aforementioned drawbacks in utilizing FRP composites for rehabilitating RC beams may be the employment of cementitious matrix in place of epoxy, thus resulting in the substitution of FRP with FRCM composites. This material has been used recently in the flexural retrofitting of RC beams [9–12].

Fédération internationale du béton (fib) Bulletin 14 [18] and ACI 440.2R-17 guidelines [20] have classified the failure modes of RC beams upgraded in flexure using externally bonded FRP sheets into two general categories: where the full composite action is generated, and where premature debonding takes place. These are further categorized into seven different failure modes [21]. In the first category where full composite action is developed, modes of failure consist of rupture of FRP sheets preceded by yielding of tensile steel rebars, and concrete crushing in compression preceded by yielding (or non-yielding) of tensile steel rebars with undamaged FRP sheets. In the second category where premature debonding occurs, composite action between concrete and FRP is lost, prohibiting the upgraded beam from attaining its ultimate flexural resistance. Fig. 1 shows typical debonding failure modes of FRP-strengthened RC beams [8]. The first mode of failure in the second category is the concrete cover separation (Fig. 1(a)), which is the most frequently reported failure mode in the literature [21–25]. This failure mode is owing to the normal stresses generated at the ends of FRP sheets. The tensile steel rebars act as a bond breaker, and the concrete cover separates from the rest of the beam (Fig. 1(a)). Concrete cover separation is partly controlled by the stress level at the cutoff point of the FRP sheets. This failure mode can be generally alleviated via anchorage means (such as FRP U-wraps) and/or by minimizing the stress at the FRP termination point by locating the cutoff point as close to the zero-moment zone as possible [20,24,26]. Another failure mode in the second category is plate-end interfacial debonding (Fig. 1(b)), in which failure takes place in the concrete layer close to the concrete/adhesive interface. This failure mode is usually owing to high normal and interfacial shear stresses close to the FRP ends that exceed the concrete strength [22]. Plate-end interfacial debonding is uncommon and can be considered to be critical in short shear-dominated RC members. Another mode of failure in the second category is intermediate flexural crack-induced interfacial debonding (see Fig. 1(c)). In this failure mode, debonding commences at a main flexural crack within the maximum-moment zone and then spreads in the direction of the decreasing moment to the end of externally bonded FRP sheets [27]. This mode of failure is commonly known as IFC (or IC) debonding [28,29]. As seen in Fig. 1(d), debonding failure modes of FRP-upgraded RC beams may also include flexural-shear crack-induced debonding. It is a failure mode in which debonding starts at a main flexural shear crack within the shear-span zone and then spreads to the nearest end of FRP sheets. The final failure mode of FRP-strengthened RC beams is the concrete shear failure. Even though it is not a debonding failure, it is classified here as the full composite action between concrete and FRP sheets is not developed.

Raoof et al. [12] compared the flexural behavior of RC beams upgraded with externally bonded FRP and FRCM composites. Thirteen RC beams were prepared, upgraded, and tested in four-point flexure. One of the specimens was used as a control beam. Five beams were strengthened with FRP sheets, whereas seven specimens were upgraded with FRCM layers. FRCM strengthening was found to be generally inferior to the FRP system in increasing the flexural resistance of RC beams, with the effectiveness ratio between the two systems ranging from 0.46 to 0.80. Two failure modes were reported in the FRP-upgraded beams. They included fiber rupture at the maximum-moment region and flexural-shear crack-induced debonding. However, in the FRCM-upgraded beams, five different modes of failure were reported. They involved textile rupture at the maximum-moment region, debonding of FRCM composite from the concrete with peeling off parts of concrete cover, slippage of the textile rovings through the cement mortar, interlaminar debonding at the textile-matrix interface, and textile slippage at the zone where the longitudinal FRCM layers meet the FRCM U-jacket for beams with U-anchorage. These failure modes were noted to be sensitive to the textile fiber materials, the number of FRCM layers, and the textile surface condition (dry or coated fibers).

Whereas numerous research studies are available in the literature concerning flexural rehabilitation of RC beams using any of the above-mentioned techniques, work on comparing different traditional and recent techniques that were designed to provide the same flexural strength enhancement of RC beams could not be found. The prime goal of this study is to investigate the efficiency of innovative versus traditional techniques in flexural retrofitting of reinforced concrete beams. In this regard, four-point flexure tests were carried out on seven RC beams. Test matrix comprised of two control and five strengthened RC beams. Flexural strengthening schemes included bonded steel plate, externally bonded CFRP sheets, NSM steel rebars, externally bonded carbon fiber reinforced cementitious matrix (CFRCM) composite, and innovative hybrid system comprising of ultra-high performance concrete (UHPC) layer combined with NSM CFRP strips. It is worth mentioning that different strengthening systems were designed to provide approximately the same peak load as the first control beam. The peak load of the tested specimens was analytically assessed using the equations of ACI 318-19 [30] and ACI 440.2R-17 [20]. Additionally, nonlinear FE (finite element) modeling was conducted. The validated FE models were further extended for some useful parametric studies of interest.

2. Experimental study

2.1. Test specimens

Table 1 summarizes the test matrix of this study. The design of test specimens was carried out to compare between innovative and traditional techniques in flexural retrofitting of reinforced concrete beams. The test matrix consisted of seven beams divided into two control specimens (BC-1 and BC-2) and five strengthened beams (BS1 to BS5). It should be clarified that this study represents the practical problem of flexural strengthening of RC beams having internally corroded tension reinforcement. The goal was to investigate the efficacy

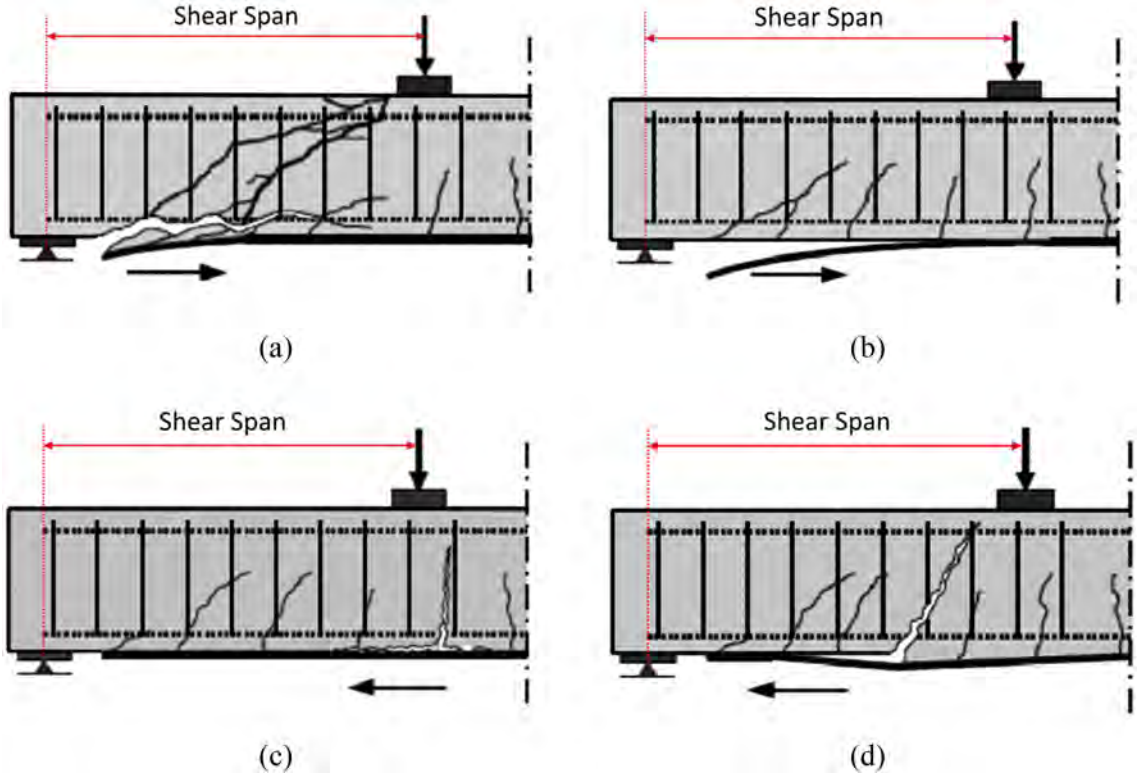

Fig. 1. Debonding failure modes of FRP-upgraded RC beams [8]: (a) Concrete cover separation; (b) Plate-end interfacial debonding; (c) Intermediate flexural crack debonding; (d) Flexural-shear crack debonding.

Table 1
Details of test matrix.

Beam ID	Strengthening system	Novelty of strengthening system	No. of specimens
BC-1	Unstrengthened		1
BC-2	Unstrengthened		1
BS1	Bonded steel plate (thickness = 5 mm)	Old and traditional	1
BS2	2 layers of externally bonded CFRP composite	Old and traditional	1
BS3	2ϕ16 mm NSM steel rebars	Old and traditional	1
BS4	2 layers of externally bonded carbon fiber reinforced cementitious matrix (CFRCM) composite	Recent and uncommon	1
BS5	Hybrid UHPC combined with NSM CFRP strips	Innovative	1
Total number of beam specimens			7

of different strengthening systems at restoring the original flexural capacity of deficient beams. To achieve this goal, two control beams were designed. The first control beam (BC-1) signifies the original beam without corroded reinforcement. However, the second control beam (BC-2) represents the deficient beam with corroded tension steel rebars. The strengthening systems of beams BS1 to BS5 were designed to provide flexural capacity enhancement equal nearly to the difference between flexural capacities of control beams BC-1 and BC-2.

All specimens were prismatic with dimensions of 200 × 400 × 2800 mm (width × depth × span). Details of the unstrengthened control specimens BC-1 and BC-2 are depicted in Fig. 2. The first control specimen BC-1 was constructed with 3ϕ16 mm steel rebars as tension reinforcement and 2ϕ10 mm steel rebars as top reinforcement. Transverse reinforcement of ϕ8 mm stirrups at a center-to-center spacing of 140 mm was used all over the span. The reinforcement represented typical beams in RC buildings, and this specimen was used as a baseline for comparison with strengthened beams. In designing of control beam BC-2, two-thirds of the main tension steel rebars of specimen BC-1 were assumed to have corroded. Control beam BC-2 was designed to be deficient in flexure with 1ϕ16 mm as longitudinal tension steel, which gives a steel ratio close to the minimum codified limits [30]. However, top steel and stirrups of BC-2 were identical to BC-1.

The strengthened specimens were similar to the second control beam, but they were upgraded with different techniques. As depicted in Table 1, the first strengthened beam BS1 was upgraded with an externally bonded ASTM A36 steel plate of 5 mm thickness. This plate was adhesively attached to the bottom side of the beam with the help of Sika-31 (structural two-component adhesive and repair mortar, based on a combination of epoxy resins and special fillers). Besides, in order to alleviate the concrete cover separation at the plate ends, four high strength threaded rods were used to connect the plate ends to the concrete (see Fig. 3). The application of the strengthening system initially involved sandblasting of the bottom side of the beam to remove dirt and any loose material. Four holes at the end of the plate were first driven at a center-to-center spacing of 100 mm in the concrete beam. Subsequently, four steel rods of 10 mm diameter were planted into the holes with the help of Sika-31. The plate was then bonded to the bottom side of the concrete beam using Sika-31. After the setting of Sika-31, nuts were inserted and tightened on the rods to aid in firmly anchoring the plate to the concrete surface (see Fig. 3).

The second upgrading system involved external bonding of two CFRP layers to the bottom side of specimen BS2, as seen in Fig. 3. In order to inhibit end debonding and concrete cover delamination at the end of CFRP sheets, two layers of CFRP U-wrap were added at the end of the longitudinal CFRP sheets (Fig. 3). Application of CFRP sheets followed the standard procedure as recommended by the man-

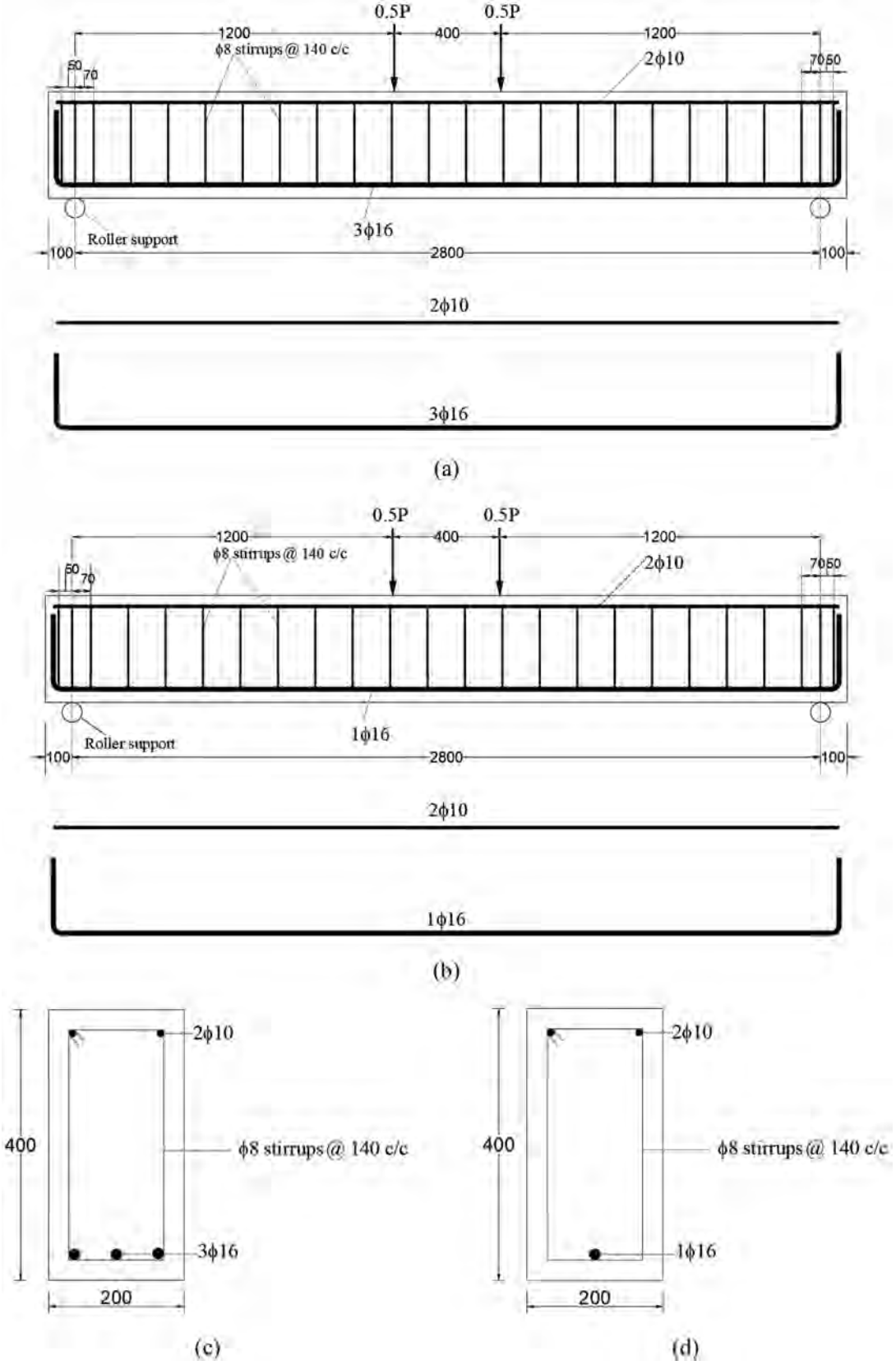

Fig. 2. Dimensions and reinforcement detailing of control beams (Note: All dimensions are in mm): (a) Elevation of BC-1; (b) Elevation of BC-2; (c) Mid-span section of BC-1; (d) Mid-span section of BC-2.

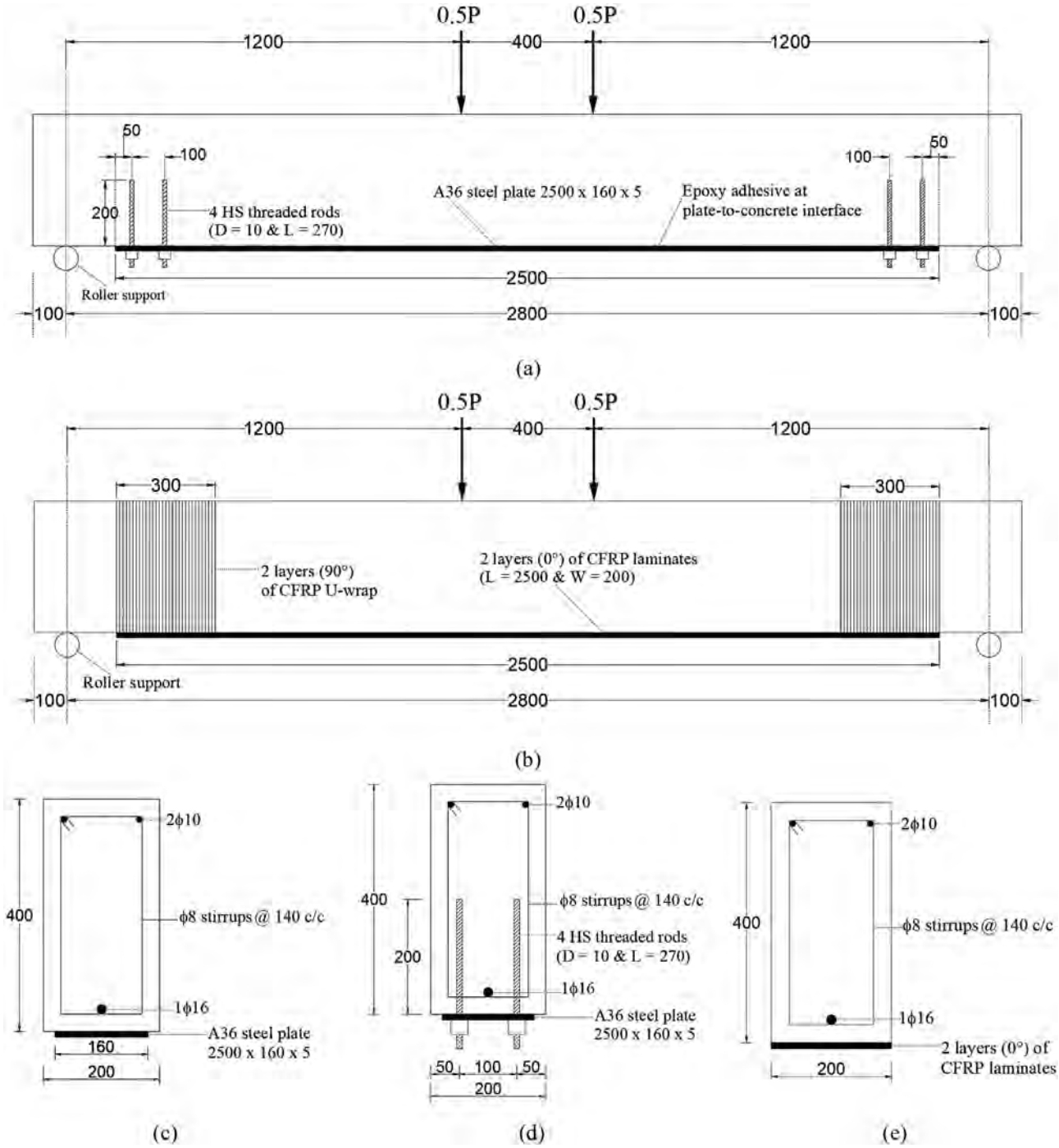

Fig. 3. Details of strengthened beams BS1 and BS2 (Note: All dimensions are in mm): (a) Elevation of BS1; (b) Elevation of BS2; (c) Mid-span section of BS1; (d) Section of BS1 at end of steel plate; (e) Mid-span section of BS2.

ufacturer and the guidelines of Ref. [20] utilizing the wet layup method after proper surface preparation.

Details of strengthening scheme for specimen BS3 are shown in Fig. 4. This beam had 2ϕ16 mm NSM steel rebars placed in grooves that were filled with Sika-31. These grooves had dimensions of 40 × 30 mm along the tension side in the bottom concrete cover. The grooves were roughened using sandblasting and then cleaned. Two layers of Sika-31 were applied into the grooves. After the first layer was applied, the steel rebars were inserted, and then the second layer of Sika-31 was added. Subsequently, the adhesive and repair mortar (Sika-31) was leveled with the concrete surface.

As illustrated in Table 1 and Fig. 4, the fourth strengthening system (specimen BS4) incorporates external bonding of two layers of CFRCM composite to the tension side of the beam. The design of BS4 was the same as BS2 except with the replacement of the two-part epoxy-based impregnating resin (Sika-300) used in BS2 with commercially available polymer-modified cementitious mortar. After proper surface preparation similar to specimen BS2, a mortar layer of approximately

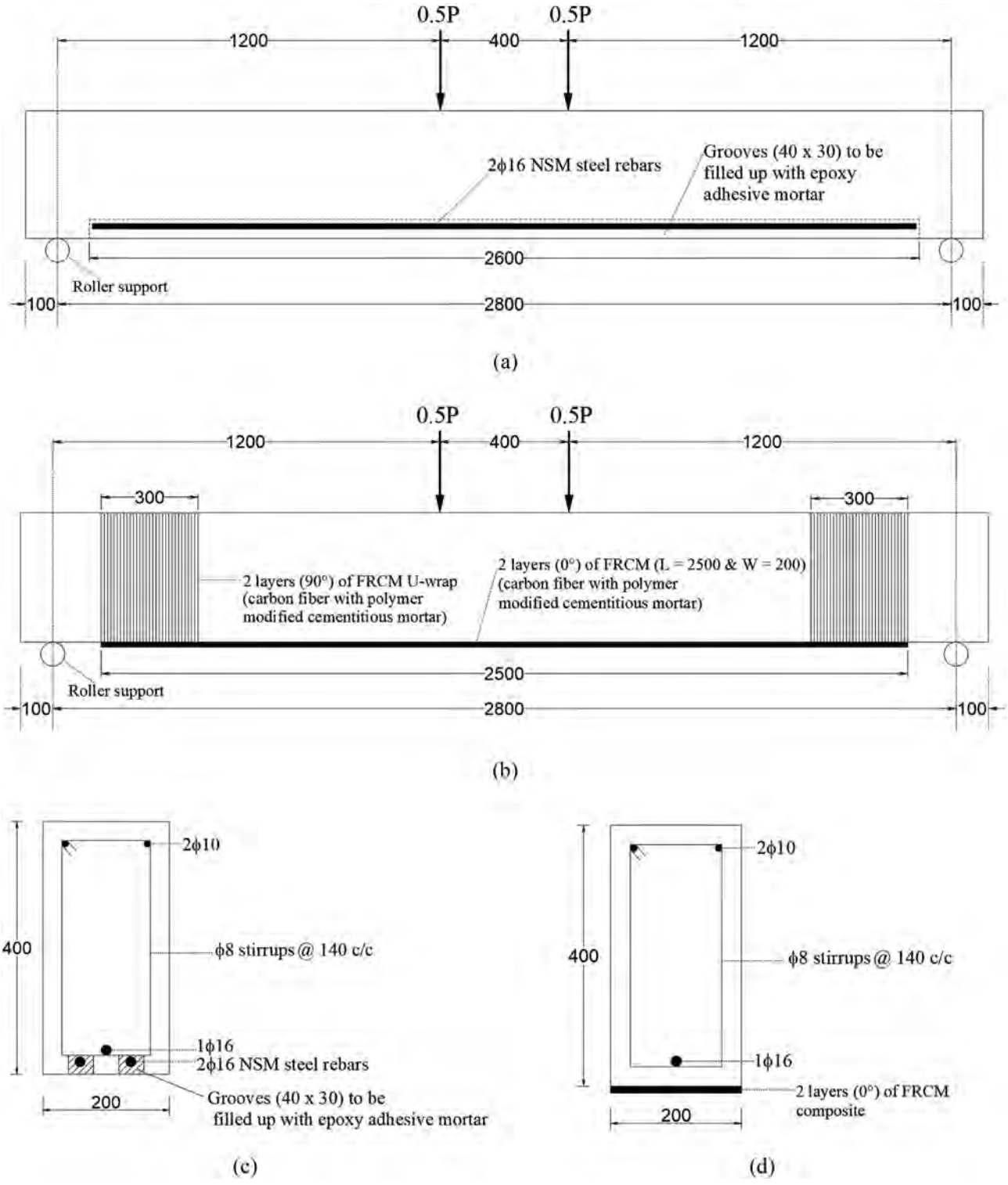

Fig. 4. Details of strengthened beams BS3 and BS4 (Note: All dimensions are in mm): (a) Elevation of BS3; (b) Elevation of BS4; (c) Mid-span section of BS3; (d) Mid-span section of BS4.

2 mm thickness was applied onto the bottom surface of the beam. Then, the first carbon fiber layer was slightly pressed into the mortar layer. The first carbon fiber layer was fully covered by the second layer of mortar, and the steps were repeated for the second carbon fiber layer.

The last specimen BS5 was strengthened with an innovative system comprising of the UHPC layer - added to the compression side of the beam - combined with NSM pultruded CFRP strips, as seen in Fig. 5 and Table 1. The installation procedure involves cutting two grooves with dimensions 2800 × 50 × 30 mm along the compression side in the top concrete cover. Similar to specimen BS3, grooves were roughened using sandblasting and then cleaned. Then two layers of Sika CarboDur CFRP plates of 50 mm width were inserted in each groove and glued to the concrete using Sika-30 (two-component,

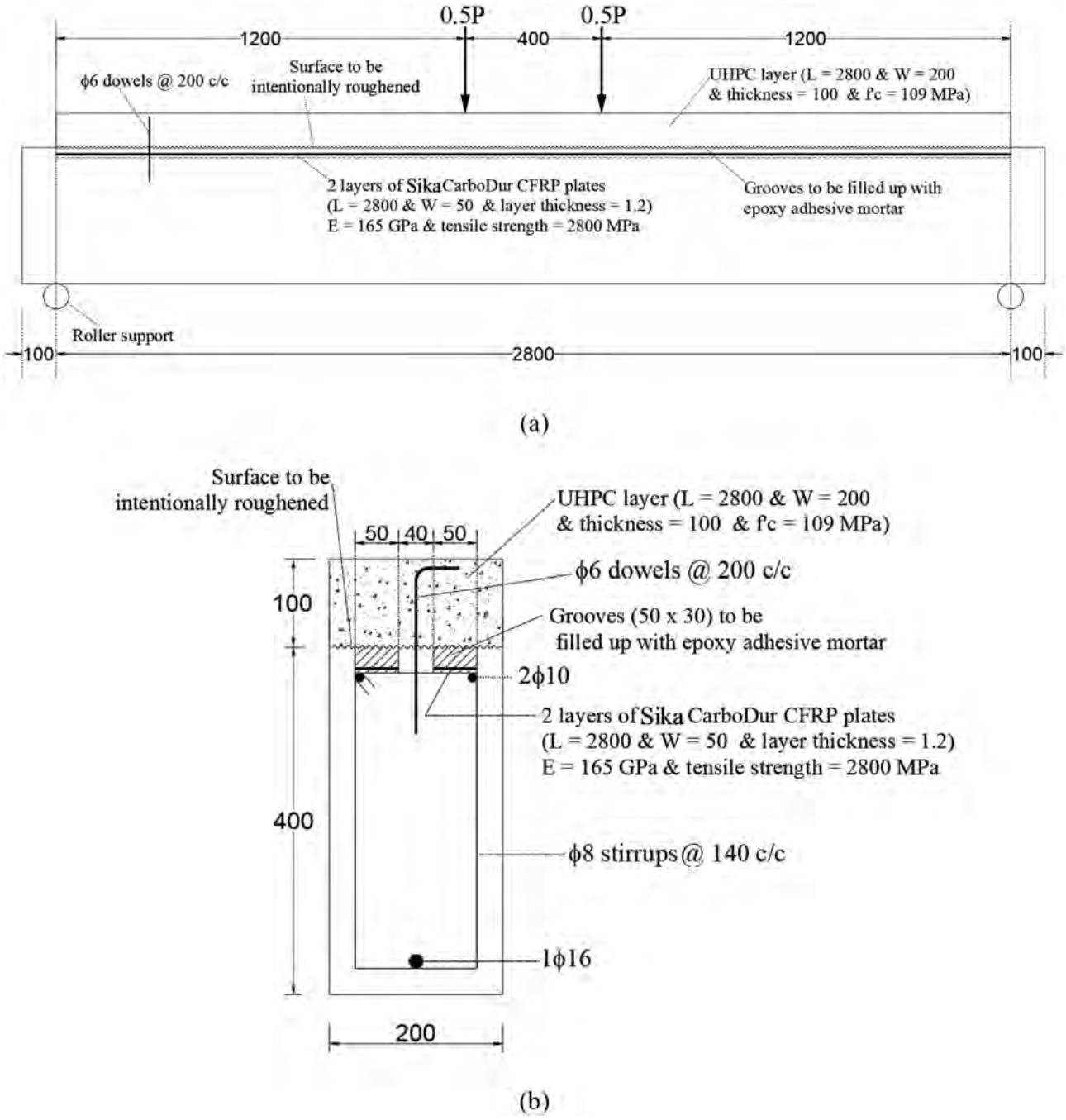

Fig. 5. Details of strengthened beam BS5 (Note: All dimensions are in mm): (a) Elevation; (b) Mid-span section.

high-modulus, high-strength, structural epoxy paste adhesive). After curing of Sika-30, epoxy adhesive and repair mortar (Sika-31) was used to fill out the grooves, and the mortar was leveled with adjacent concrete, and then it was left for curing. The top surface of the concrete beam was then intentionally roughened, and ϕ6 mm dowels at a center-to-center spacing of 200 mm were planted into the top side of the concrete beam using a special mortar grout (Fig. 5). After cleaning the top beam surface, a bonding agent was applied, and a thin UHPC layer of 100 mm thickness was cast onto the top side of the beam, and then it was left for curing. It should be noted that in this system and by using the UHPC layer at the top of the beam, the neutral axis depth at the ultimate state will be located in this layer, thus putting the NSM CFRP strips in tension. Therefore, the flexural capacity of the strengthened section will come from three components: the tensile force of the bottom original steel rebars, the tensile force of the top original steel rebars, and the tensile force of the added NSM CFRP strips.

2.2. Material Properties

Table 2 lists material properties employed in the preparation of specimens. The average strengths (on the testing day of beams) of both ready-mix concrete and UHPC were attained by compression testing of standard cylinders (150 × 300 mm) as per Ref. [31], and they were, respectively, 28 and 109 MPa. For cementitious mortar utilized for CFRCM strengthening of beam BS4, the compressive strength on the day of the test was measured by testing standard 50-mm cubes as per Ref. [32]. The structural two-component adhesive and repair mor-

Table 2
Properties of materials utilized in the FE modeling.

Concrete-like materials	*Concrete*	*Epoxy mortar for NSM strengthening*	*Mortar for FRCM strengthening*	*UHPC for UHPC/NSM system*		
Material model	Type 159					
Density (kg/m^3)	2320					
Compressive strength (MPa)	28	65	56.4	109		
Rate effects option	0 (Rate effects model turned off)					
Erosion factor	1.05	1.1	1.1	1.1		
Pre-existing damage parameter	0.0 (No pre-existing damage)					
Max aggregate size, DAGG (mm)	10	5	5	5		
Steel rebars, threaded rods & plates	*ϕ8*	*ϕ10*	*ϕ16*	*ϕ20*	*Threaded rods*	*Plates*
Material model	Type 24					
Density (kg/m^3)	7850					
Elastic modulus (GPa)	200					
Poisson's ratio	0.3					
Yield stress (MPa)	488	547	578	578	350	260
Tangent modulus (MPa)	0	880	862	862	0	0
Plastic strain to failure (%)	12.76	12.67	11.66	11.66	19.83	19.87
Composite material	*CFRP sheets*	*PBO textile*	*CFRP strips*			
Material model	Type 54–55					
Density (kg/m^3)	1740	880	1600			
Thickness per layer (mm)	1	0.0455	1.2			
Tensile modulus in long. dir. (GPa)	82	270	165			
Tensile modulus in transverse dir. (GPa)	3.6	270	7.25			
Longitudinal tensile strength (MPa)	834	5800	2800			
Transverse tensile strength (MPa)	83.4	5800	280			
FRP rebars	*ϕ16 GFRP rebars*	*ϕ13 CFRP rebars*				
Material model	Type 24					
Bar diameter (mm)	15.9	12.7				
Density (kg/m^3)	2158	1468				
Tensile modulus (GPa)	46	124				
Poisson's ratio	0.26	0.26				
Yield stress (MPa)	724	2068				
Tangent modulus (MPa)	0	0				
Plastic strain to failure (%)	1.00E-05	1.00E-05				

tar (Sika-31) was used for filling the grooves of NSM rebars in beam BS3. Table 2 lists the compressive strength of Sika-31 as given by the manufacturer. The steel rebars of all diameters were tested in tension following the test standard in Ref. [33] and the mechanical properties obtained through these tests are listed in Table 2. For the steel plate used for strengthening of beam BS1, standard coupons were prepared and tested according to Ref. [34]. Table 2 provides the average measured yield strength of the steel plate. For CFRP sheets and pultruded CFRP strips, tensile tests according to the relevant test standard [35] were performed on test coupons, and the average values are reported in Table 2.

2.3. Test protocol

Fig. 6 illustrates the test setup and sensor layout for unstrengthened beams and samples of upgraded specimens. As presented in Fig. 6, beams were tested under 4-point bending using a 2000-kN testing machine, which applied two-point loads on the specimens via a rigid steel beam. The load cell was employed for load measurement and the beams were tested using a displacement controlled loading strategy at a rate of 0.017 mm/s. As seen in Fig. 6, downward deflections of test beams were measured using LVDTs (Linear Variable Displacement Transducers). Additionally, strains were measured for steel rebars and strengthening systems (e.g., steel plate, CFRP sheets, NSM steel rebars, NSM CFRP strips) with the help of strain gages as presented in Fig. 6.

3. Discussion of test results

Tables 3 and 4 summarize the experimental results of the seven tested beams. It is worth noting here that the ultimate state in Table 4 corresponds to the state at which the drop of peak load reaches 20% as per Ref. [36]. It is also worth mentioning that the energy ductility index presented in Table 4 is estimated from Ref. [37] using the following formula:

$$\mu_E = \frac{E_u}{2E_y} + 0.5 \quad (1)$$

where E_y and E_u are the dissipated energy of the beam specimen at yielding of tension steel rebars and ultimate state, respectively. Figs. 7 and 8, respectively, show load–deflection plots and failure modes for test specimens.

As displayed in Fig. 7, the unstrengthened beams BC-1 and BC-2 depicted the typical response of tension-controlled beams. Flexural failure was developed due to the formation of wide vertical cracks at mid-span, and later it was followed by concrete crushing at the top side as presented in Fig. 8(a) and (b). For strengthened beam BS1, flexural cracks were initially formed in the constant-moment region until the major flexural crack caused interfacial debonding at the steel plate-to-concrete interface, like the IC (intermediate crack) debonding usually found in FRP-strengthened slabs and beams [8,28], as previously outlined in Sec. 1. This interfacial debonding occurred at a peak load of 151 kN before the onset of yielding in the main steel rebar, as shown

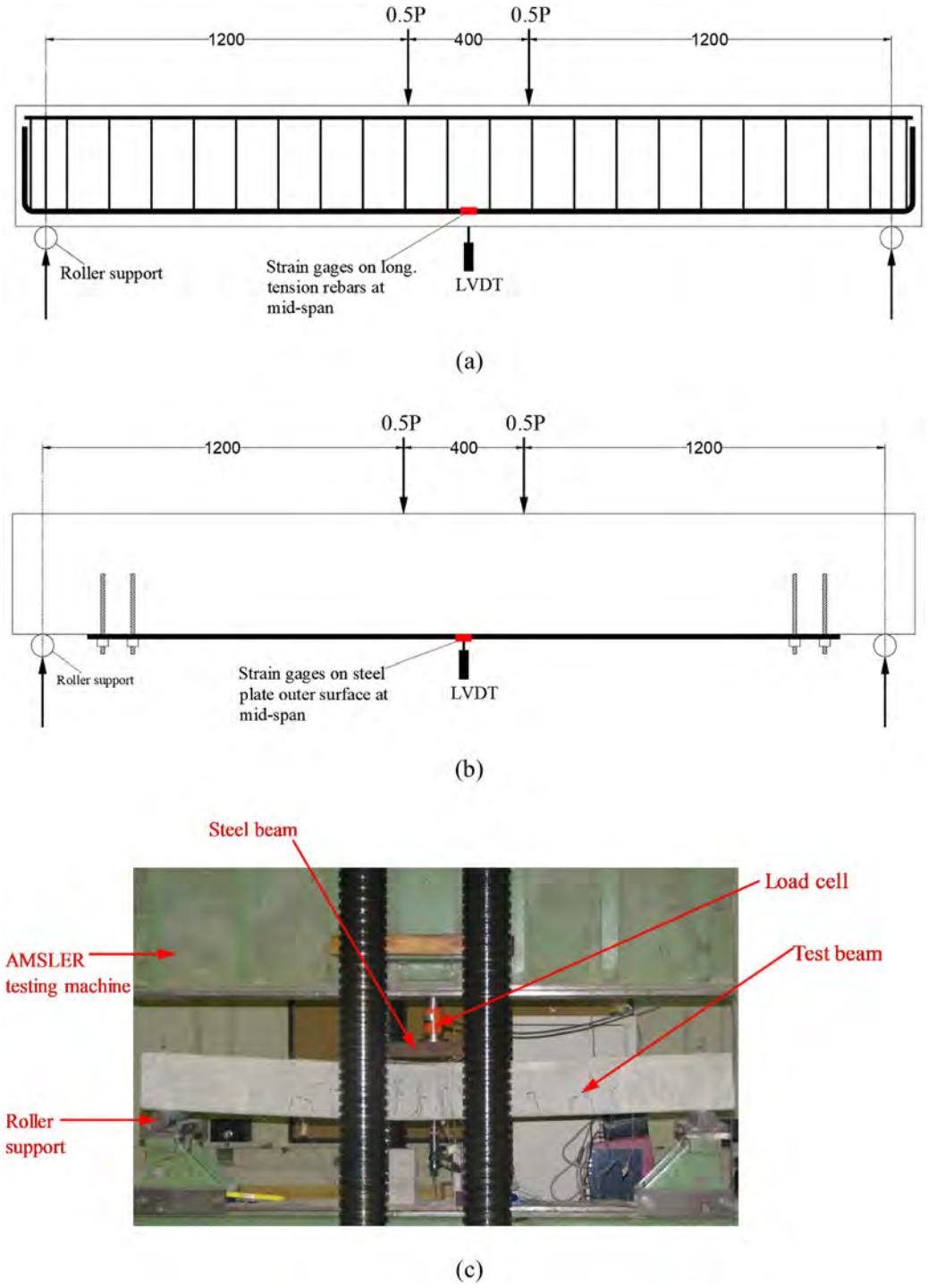

Fig. 6. Instrumentation layout and setup (Note: All dimensions are in mm): (a) Location of sensors for control beams; (b) Location of sensors for strengthened beam BS1; (c) Test setup.

in Tables 3 and 4. After steel plate debonding, the load dropped suddenly to a value of about 70 kN, and the behavior was then close to that of unstrengthened specimen BC-2. The CFRP-strengthened beam BS2 had yielding of the main steel rebar at a load of 105 kN, as seen in Table 3. At the peak load of 151 kN, failure occurred suddenly owing to IC debonding, which initiated at the bottom edge of the main flexural crack in the maximum-moment zone. Then, this debonding spread towards the roller support, as shown in Fig. 8(d). For beam BS3 strengthened with 2ϕ16 mm NSM steel rebars, the behavior was almost identical to the control specimen BC-1 (see Fig. 7) until a mid-span deflection of about 44 mm (corresponding to a vertical load of about 196 kN) at which sudden failure occurred. This was owing to the delamination of the concrete cover in the shear span near the right support (see Fig. 8(e)). This cover delamination resulted from the termination of the NSM rebars in a high shear stressed zone with diagonal shear cracks where the provided stirrups were insufficient to control the propagation of these cracks at the rebars cutoff point. For CFRCM-strengthened beam BS4, and because of the continuous nature of the carbon fibers used, the cementitious matrix lacked the ability to impregnate the fibers. Then, the proper formation of the composite

Table 3
Comparison of yield and ultimate loads for tested beams*

Beam ID	Yield load (P_y) (kN)						Ultimate load (P_u) (kN)					
	EXP	FE	AN	EXP/FE	EXP/AN	FE/AN	EXP	FE	AN	EXP/FE	EXP/AN	FE/AN
BC-1	179	197	183	0.91	0.98	1.08	204	202	184	1.01	1.11	1.10
BC-2	55	62	64	0.89	0.86	0.97	80	74	66	1.09	1.21	1.11
BS1	NY	NY	178	–	–	–	151	162	189	0.93	0.80	0.86
BS2	105	117	131	0.89	0.80	0.90	151	160	170	0.94	0.89	0.94
BS3	178	171	192	1.04	0.93	0.89	199	202	194	0.98	1.03	1.04
BS4	64	78	131	0.82	0.49	0.60	82.7	82.1	170	1.01	0.49	0.48
BS5	78.4	83.3	91	0.94	0.86	0.92	165.7	173.2	167	0.96	0.99	1.03

*EXP = experimental; FE = finite element; AN = analytical.

Table 4
Comparison of measured and FE load–deflection response for tested specimens*

Beam ID	Results	Δ_y (mm)	Δ_u (mm)	K_s (kN/m)	E_u (kN.m)	μ_Δ	μ_E	ε_{su} (με)**	$\varepsilon_{stm,u}$ (με)**	Failure mode
BC-1	EXP	10.8	76.6	16,563	13.89	7.1	6.6	***58,236***	–	SY-CC
	FE	11.4	73.2	17,302	13.75	6.4	5.8	***62,234***	–	SY-CC
	EXP/FE	0.95	1.05	0.96	1.01	1.10	1.14	0.94	–	
BC-2	EXP	6.7	89.9	8156	6.45	13.3	14.6	NA	–	SY-CC
	FE	6.2	83.0	10,032	5.82	13.5	13.1	***88,092***	–	SY-CC
	EXP/FE	1.09	1.08	0.81	1.11	0.99	1.12	–	–	
BS1	EXP	NY	5.6	27,012	0.51	–	–	1335	***1477***	DB-CC
	FE	NY	6.2	26,117	0.61	–	–	1460	***1541***	DB-CC
	EXP/FE	–	0.90	1.03	0.84	–		0.91	0.96	
BS2	EXP	8.5	19.5	12,321	2.02	2.3	2.5	***13,760***	4699	SY-DB-CC
	FE	9.3	19.5	12,639	2.04	2.1	2.3	***15,877***	4741	SY-DB-CC
	EXP/FE	0.92	1.00	0.97	0.99	1.09	1.11	0.87	0.99	
BS3	EXP	11.7	44.7	15,136	7.57	3.8	3.5	NA	NA	SY-DL-CC
	FE	9.7	42.4	17,600	7.50	4.4	4.2	***44,217***	***33,358***	SY-DL-CC
	EXP/FE	1.21	1.05	0.86	1.01	0.87	0.84	–	–	
BS4	EXP	7.785	89.8	8191	6.62	11.5	7.5	NA	551	SY-DB-CC
	FE	9.2	89.7	8430	6.71	9.7	6.7	***76,559***	554	SY-DB-CC
	EXP/FE	0.84	1.00	0.97	0.99	1.19	1.11	–	0.99	
BS5	EXP	6.0	82.6	13,154	10.93	13.9	19.0	NA	9799	SY-CC
	FE	5.0	86.7	16,614	12.46	17.3	20.2	***99,710***	10,558	SY-CC
	EXP/FE	1.19	0.95	0.79	0.88	0.80	0.94	–	0.93	

*Δ_y = mid-span deflection at yielding of main steel; Δ_u = mid-span deflection at ultimate state; K_s = effective pre-yield stiffness; E_u = energy dissipated at ultimate state; μ_Δ = deflection ductility ratio = Δ_u/Δ_y; μ_E = energy ductility as calculated from Eq. (1); ε_{su} = ultimate strain of main tension steel rebars at mid-span; $\varepsilon_{stm,u}$ = ultimate strain of strengthening material at mid-span; SY-CC = steel yielding followed by concrete crushing at mid-span; DB-CC = intermediate crack debonding followed by concrete crushing at mid-span; SY-DB-CC = steel yielding at mid-span followed by intermediate crack debonding and finally concrete crushing at mid-span; SY-DL-CC = steel yielding at mid-span followed by concrete cover delamination at end of NSM rebars and finally concrete crushing at mid-span; NY = No steel yielding; NA = not available data.
**Values in italic bold font indicate steel yielding.

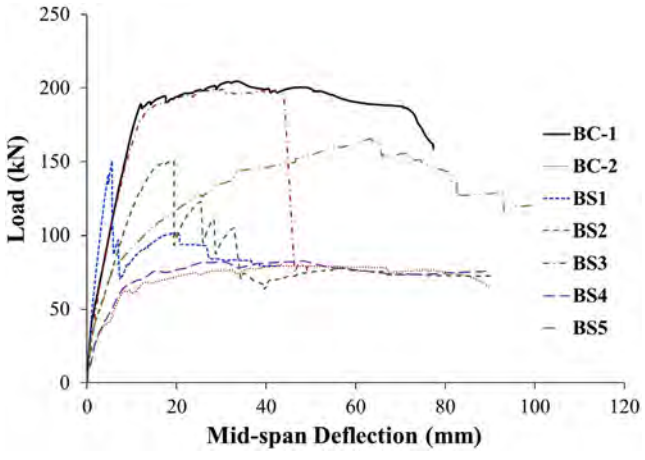

Fig. 7. Load-deflection plots for test specimens.

action between the matrix and the fiber sheets was mitigated. Thus, upon yielding of tension steel rebars and the appearance of the first flexural crack, sudden debonding occurred at the fibers-to-matrix interface [1,38], as seen in Fig. 8(f) and the behavior of the beam was then almost similar to the control specimen BC-2, as seen in Fig. 7. For beam BS5 that was strengthened using the innovative hybrid UHPC/NSM technique, steel yielding occurred in the main steel rebars at a load of about 78 kN followed by large flexural cracks in the maximum-moment zone (see Fig. 8(g)). These cracks propagated upwards till the UHPC layer, thus mobilizing the contribution of both top steel rebars and NSM CFRP strips in enhancing the flexural resistance of the beam section. The ultimate failure mode was due to the crushing of the UHPC layer at a deflection of about 99 mm, as illustrated from Fig. 7.

Fig. 9(a) to (c) show the impact of the retrofitting system on the behavior of test specimens with regard to percent increase (over control beam BC-2) in flexural strength, effective flexural stiffness, and dissipated energy, respectively. Values for control beam BC-1 are also indicated in the figures for comparison. Even though the five strengthening systems were designed to give approximately the same flexural strength, their behavior was different. As seen in Fig. 9(a), the best flexural strength enhancement was provided by NSM steel rebars, with a 149% strength increase, which was very close to the control beam BC-1. Both steel plate and externally bonded CFRP sheets gave the same flexural capacity enhancement (88%), which was considerably

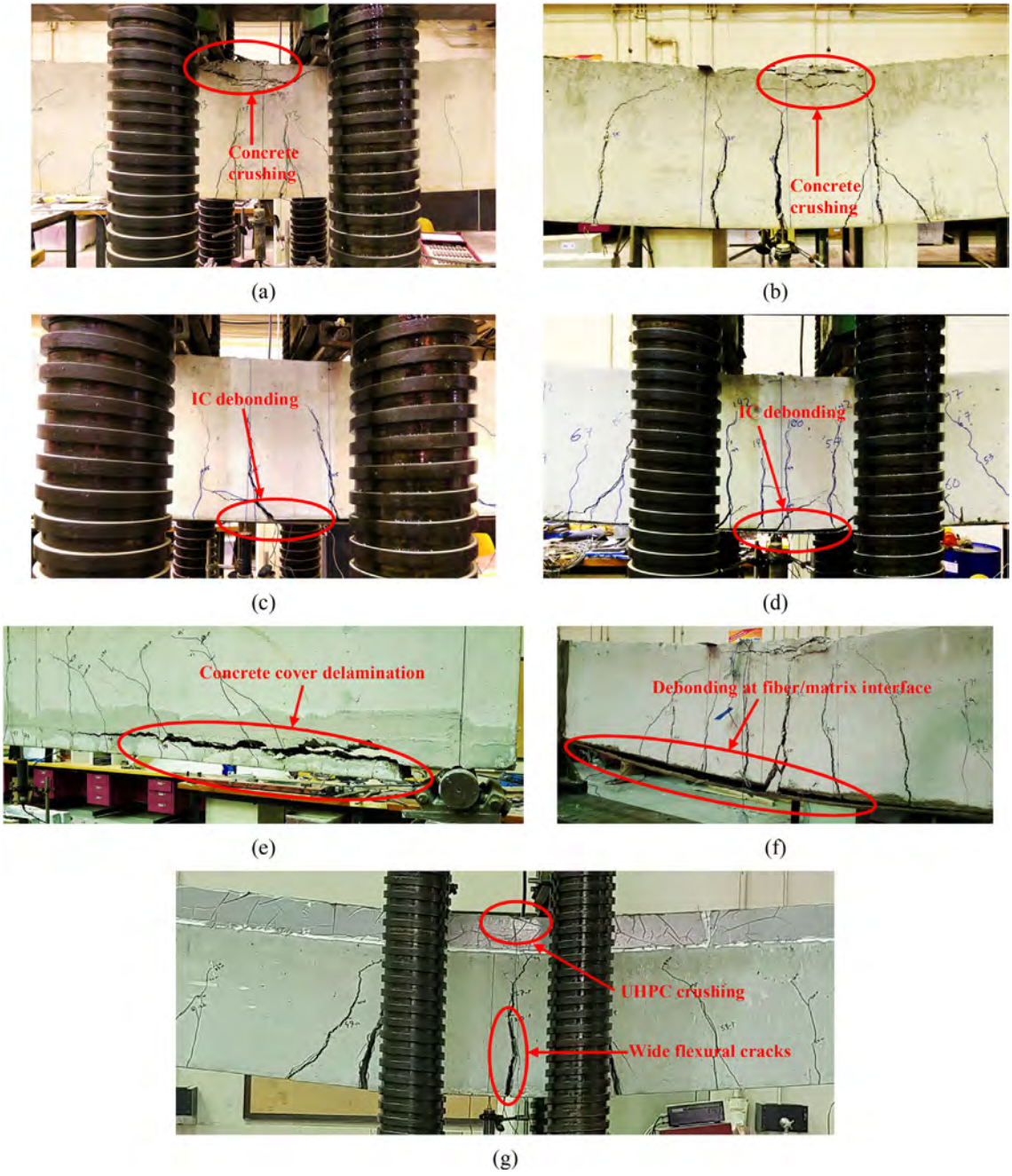

Fig. 8. Failure modes for beams: (a) BC-1; (b) BC-2; (c) BS1; (d) BS2; (e) BS3; (f) BS4; (g) BS5.

below the 155% enhancement for BC-1. Due to the loss of the composite action, externally bonded CFRCM layers had almost no improvement in flexural strength (=3%). The innovative system of hybrid UHPC/NSM CFRP strips had a 107% strength enhancement that was about 70% of the flexural capacity increase provided by control specimen BC-1. Regarding the increase in effective flexural stiffness, Fig. 9 (b) depicts that the steel plate was the most effective by increasing the stiffness by 231% (over that of unstrengthened beam BC-2), which was about 2.24 times the stiffness gain in the control beam BC-1. However, as shown in Fig. 9(c), the best strengthening system in terms of enhancing energy dissipation at the ultimate state is the hybrid UHPC/NSM technique that provided 69% enhancement. Both steel plate and CFRP strengthening had resulted in a substantial reduction in the energy dissipation due to the sudden IC debonding.

In conclusion, with respect to the failure mode and the load–deflection characteristics, the best performance was given by the innovative hybrid strengthening technique owing to its ductile behavior. This system also gave a balanced behavior for the three response parameters (strength, stiffness, and energy dissipated). In order of diminishing performance level, this system is followed by NSM steel rebars, CFRP sheets, steel plate, and finally, CFRCM strengthening. Even though Toutanji and Deng [11] used successfully continuous carbon fiber sheets along with inorganic matrix to enhance the flexural resistance of RC beams, it is not recommended to utilize continuous fiber sheets with cementitious matrix due to the disability of the matrix to impregnate the fibers and hence the lack of the composite action. In addition, in order to alleviate the sudden concrete cover delamination failure mode noticed in beam BS3, it is recommended

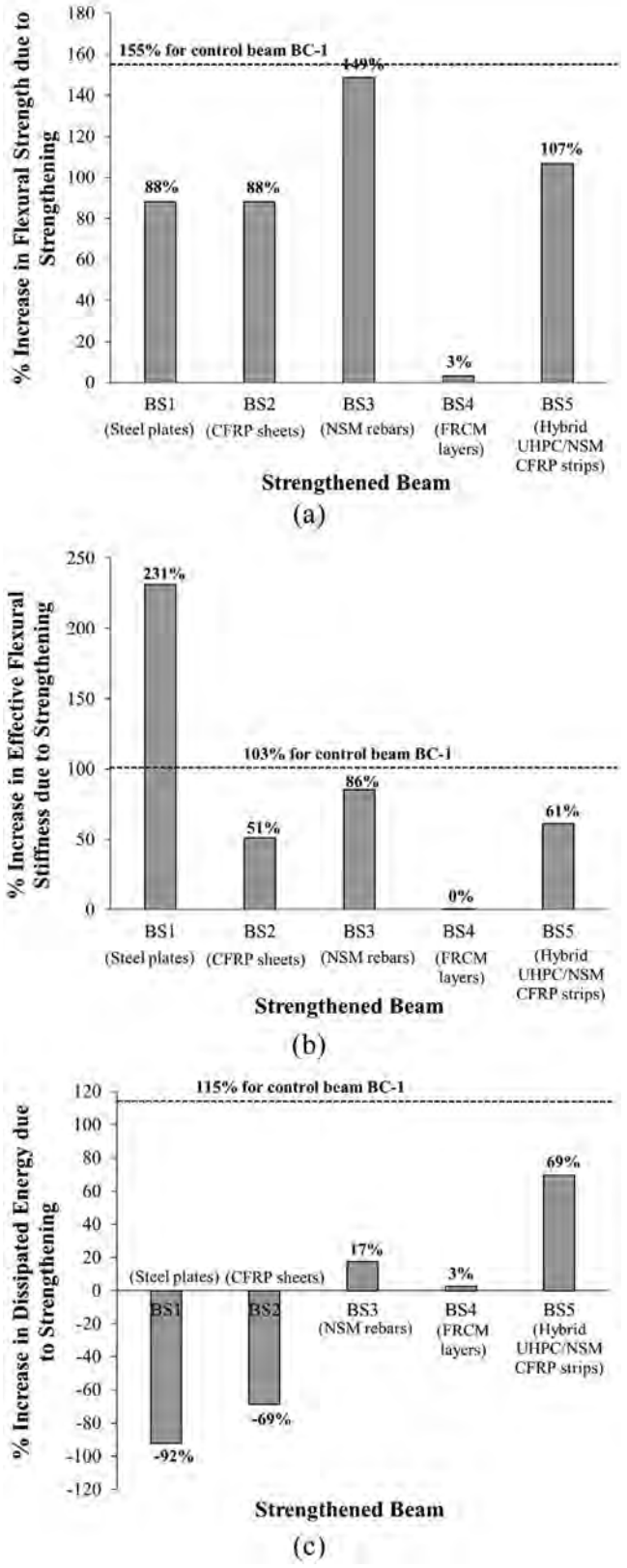

Fig. 9. Effect of strengthening system on behavior of beams with respect to: (a) Flexural strength enhancement; (b) Increase in effective stiffness; (c) Increase in dissipated energy.

to check the shear capacity at the cutoff points of the NSM rebars as per ACI 318-19 [30] and provide external shear strengthening at those locations, if needed.

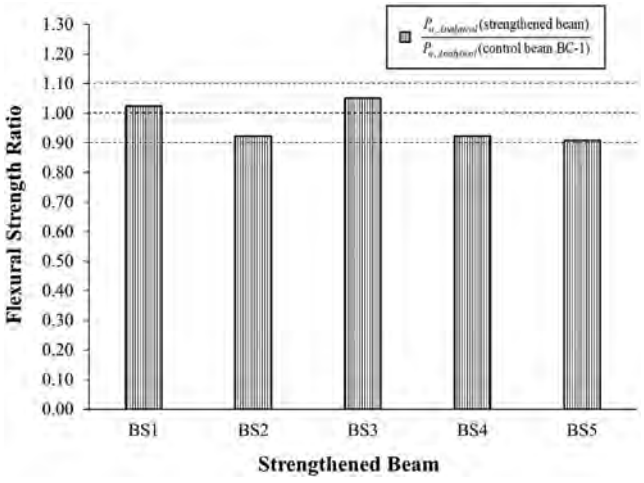

Fig. 10. Comparison of analytical prediction of ultimate load of strengthened beams with control specimen BC-1.

The innovative system of hybrid UHPC/NSM CFRP strips may be thus recommended in real applications. However, its use may be limited to cases where it is required to increase the positive moment capacity of roof beams in which the bottom side is inaccessible, or the increase in the beam depth below the slab is not practically feasible. This system may also be used for typical floor beams but with limiting the thickness of the UHPC layer such that it can be embedded in the flooring. In such a case, the width of the added UHPC layer may be more than the web width of the beam in order to compensate for the limited layer depth. There exists another vital concern if this strengthening technique is recommended in real practice. The wide flexural cracks observed for BS5 brings our attention to the necessity of checking the crack control requirements at the service load level - as per the provisions of current codes of practice - for original steel rebars closest to the bottom beam surface.

4. Analytical modeling

A simple approach was used to design the strengthening systems by assessing the flexural capacity of test specimens and ensuring that the ultimate load of upgraded beams will become in close agreement with that of control specimen BC-1. With the assumption of the perfect bond at the concrete/steel rebars interface, the ACI 318-19 code [30] was employed to calculate the yield and ultimate capacities of control specimens and strengthened beam BS3. For strengthened beam BS1, a perfect bond was assumed at the concrete/steel plate interface, and the ACI 318-19 code [30] was also employed to assess both yield and ultimate strengths. For strengthened specimens BS2 and BS4, the procedure of the ACI 440.2R-17 guidelines [20] was followed to assess the yield and ultimate capacities, assuming IC debonding at CFRP (or CFRCM) to the concrete interface. It should be noted that the contribution of mortar was ignored while assessing the yield and ultimate strengths of specimen BS4. As slippage of NSM CFRP strips was not noticed for beam BS5, calculation of the flexural capacity of the beam was conducted assuming perfect bond at NSM CFRP strips/concrete interface. Both ACI 318-19 and ACI 440.2R-17 were followed to compute the yield and ultimate moments of the cross-section of strengthened beam BS5.

It is worth noting that in the analytical prediction of the flexural strength of specimens, a strength reduction factor of one ($\phi = 1$) was used. Table 3 summarizes the analytical predictions of both yield and ultimate loads of test specimens along with a comparison with test results. Fig. 10 presents a comparison of the analytical prediction of the peak load of upgraded beams with unstrengthened specimen BC-1. It is noted from Table 3 and Fig. 10 that the analytically predicted peak load of retrofitted specimens became in close agreement with

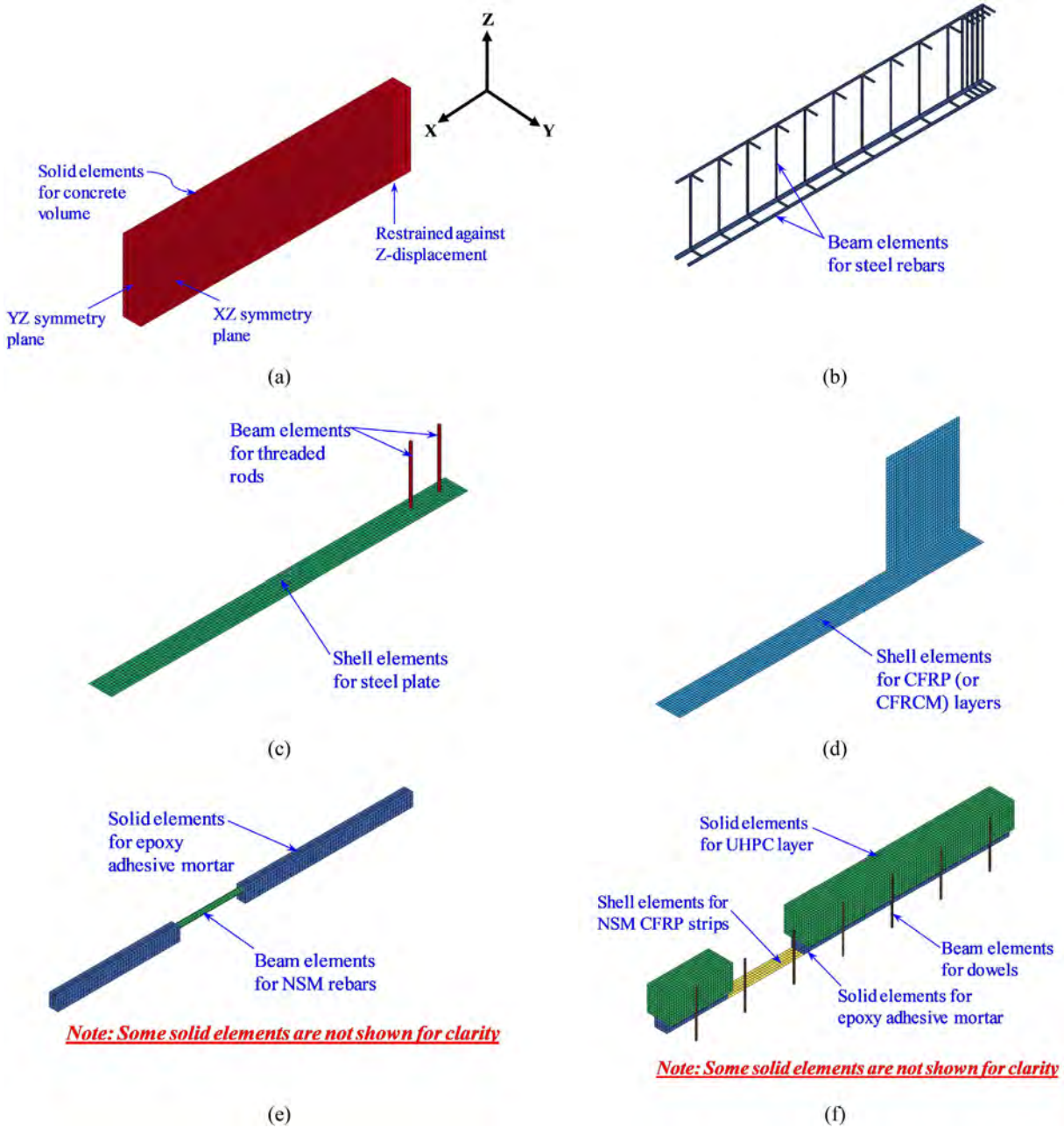

Fig. 11. FE model for one-quarter of beams: (a) Concrete for BC-1 & BC-2; (b) Steel rebars for BC-1; (c) Strengthening system for BS1; (d) Strengthening system for BS2 & BS4; (e) Strengthening system for BS3; (f) Strengthening system for BS5.

that of control beam BC-1 with the ratio $\frac{P_{u,Analytical}(\text{strengthened beam})}{P_{u,Analytical}(\text{control beam BC - 1})}$ ranging from 0.91 to 1.05. As evidenced from Table 3, due to the very poor performance of the CFRCM composite system and the premature debonding at fibers-to-matrix interface observed in the experiment, the guidelines of the ACI 440.2R-17 excessively overestimated the ultimate capacity of specimen BS4 by giving tested-to-predicted peak load ratio of 0.49. For control specimens, the analytical prediction underestimated the ultimate load by 11 to 21%. For steel-plated specimen BS1, the analytical modeling predicted yielding in the main steel rebar while this was not observed in the testing. In addition, the analytical prediction overestimated the peak load by 20%. This was attributed to the IC debonding, noticed in the testing at the plate-to-concrete interface, which has not been accounted for in the analytical model. For specimens BS2, BS3, and BS5, good agreement was achieved between the predicted and measured results with errors in the prediction of ultimate load varying from 1% to 11%, as seen in Table 3. In conclusion, the analytical approach was not able to accurately estimate the flexural resistance for all test specimens. Therefore, a more precise assessment tool is required. Nonlinear 3D FE modeling was employed as a numerical assessment approach.

5. FE modeling

LS-DYNA software [39] was employed to conduct FE modeling of specimens. One-quarter of the specimen was simulated taking advantage of its symmetry about two planes. The FE model of different parts

Table 5
Values of tensile and shear bond strength for tiebreak surface-to-surface contact of strengthened beams*

Beam ID	Tensile bond strength (σ_{nf}) (MPa)	Shear bond strength (σ_{sf}) (MPa)	Refs.
BS1	$\sigma_{nf} = 0.62\sqrt{\min(f'_c, f'_{cm})}$ $\sigma_{nf} = 0.62\sqrt{28} = 3.28$ MPa	$\sigma_{Sf} = 1.5\beta_w\sigma_{nf}$ $\beta_w = \sqrt{\frac{2.25-b_p/b_c}{1.25+b_p/b_c}} = 0.841$ $\sigma_{Sf} = 4.14$ MPa	[8,9]
BS2	$\sigma_{nf} = 0.62\sqrt{f'_c}$ $\sigma_{nf} = 0.62\sqrt{28} = 3.28$ MPa	$\sigma_{Sf} = 1.5\beta_w\sigma_{nf}$ $\beta_w = \sqrt{\frac{2.25-b_f/b_c}{1.25+b_f/b_c}} = 0.745$ $\sigma_{Sf} = 3.67$ MPa	[7,8]
BS4	Based on the work of Silfwerbrand [43] : $\sigma_{nf} = \frac{\sigma_{sf}}{3.1} = 0.143$ MPa	From model of Ombres [44], $\sigma_{Sf} = 0.443$ MPa	[43,44]
BS17 & BS18	Based on the work of Silfwerbrand [43] : $\sigma_{nf} = \frac{\sigma_{sf}}{3.1} = 1.06$ MPa	$\sigma_{nf} = 0.62\sqrt{\min(f'_c, f'_{cm})}$ $\sigma_{nf} = 0.62\sqrt{28} = 3.28$ MPa	[9,43]

*f'_c = compressive strength of concrete; f'_{cm} = compressive strength of epoxy adhesive mortar (for BS1) or cementitious matrix (for BS17 & BS18); b_p = width of steel plate; b_c = width of RC beam; b_f = width of CFRP sheet.

of specimens is illustrated in Fig. 11(a) to (f). Eight-node brick elements were utilized in meshing both concrete volume and epoxy mortar. All of the longitudinal steel rebars, stirrups, NSM steel rebars, dowels, and threaded rods were simulated utilizing two-node beam elements. Steel plate, CFRP (or CFRCM) layers, and CFRP strips were represented with 4-node shell elements of Belytschko-Tsay formulation [40]. It is worth mentioning here that cementitious mortar in specimen BS4 was not included in the FE model. The size of the FE mesh ranged from 10 to 25 mm. It should be pointed out that a numerical convergence study was conducted, and more fine-tuning of mesh size would have a slight impact on the FE results. The bond between each of: (i) steel rebars and concrete, (ii) NSM steel rebars and adhesive mortar, (iii) NSM CFRP strips and adhesive mortar, and (iv) adhesive mortar and concrete was assumed as perfect.

Table 2 lists the properties of different materials employed in the numerical modeling. Model type 159 (continuous surface cap model) was employed for solid elements of: concrete, epoxy adhesive and repair mortar (Sika-31), and UHPC layer. This material model is fully detailed in Ref. [41]. In this model, solid elements eroded when the maximum principal strain became 5% for concrete volume and 10% for both Sika-31 and UHPC layers [41]. Model type 24 (piecewise linear plasticity model) was used for longitudinal steel rebars, stirrups, steel plate, NSM steel rebars, dowels, and threaded rods. The enhanced composite damage model type 54–55 was employed for shell elements of CFRP and CFRCM composites along with Chang and Chang failure criterion [42].

As noticed from the previously discussed experimental results, IC debonding was found in specimens BS1 and BS2. Also, premature interfacial debonding was noted at the carbon fibers-to-matrix interface in beam BS4. Accordingly, for the performance prediction of these specimens, tiebreak surface-to-surface contact was input at strengthening layer-to-concrete interface in specimens BS1, BS2, and BS4. This contact permits the separation of the two initially tied surfaces as per the following formula:

$$\left(\frac{|\sigma_s|}{\sigma_{s,F}}\right)^2 + \left(\frac{|\sigma_n|}{\sigma_{n,F}}\right)^2 \geqslant 1 \quad (2)$$

where σ_s and σ_n are, in turn, the shear and normal stresses. Yet, $\sigma_{s,F}$ and $\sigma_{n,F}$ are the shear and normal stresses at failure, respectively. Table 5 lists formulas used in this study to compute tensile and shear bond strengths for tiebreak surface-to-surface contact of beams BS1, BS2, and BS4. The related references [7–9,43,44] are also given in Table 5.

Taking advantage of the symmetry in geometry, supports, and loading, one-quarter of the test specimen was simulated. As seen in Fig. 11, the roller bearing was simulated by restraining the nodal Z-displacement. The symmetry boundary conditions were assigned to the nodes on the symmetry planes. The Z-displacement of the nodes lying on the loading plane was controlled to match with the loading strategy followed in the experimental program.

6. Calibration of FE modeling

The calibration of the FE modeling was conducted with the help of the test results of the seven beams discussed above. The model validation is discussed below.

6.1. Failure modes

Fig. 12(a) to (g) present the FE modes of failure for control and strengthened beams. It is explicable that the numerically predicted modes of failure are almost matching those observed in the tests. The FE analysis confirmed the ductile behavior of control beams BC-1 and BC-2, for which flexural vertical cracks were initiated in the constant-moment region, and later it was followed by concrete crushing in the top side of the beams (see Fig. 12). As seen in Fig. 12(c) and (d), both strengthened beams BS1 and BS2 were predicted to fail due to IC debonding, which initiated in the maximum-moment region and then propagated to the beam ends. As seen in Fig. 12(e), failure of strengthened beam BS3 was because of separation of the concrete cover at the termination point of NSM steel rebars. This resulted from the development of major inclined shear cracking in the shear spans. For CFRCM-upgraded beam BS4, the FE modeling displayed a failure mode similar to the experiment, as seen in Fig. 12(f). This failure was predicted to be due to premature debonding at the carbon fibers-to-concrete interface, which is similar to the interfacial debonding at the fibers-to-matrix interface observed in the testing. For beam BS5 that was strengthened using the innovative hybrid UHPC/NSM system, the FE modeling showed large flexural cracking in the constant-moment zone (see Fig. 12(g)). These cracks propagated upwards till the UHPC layer with the ultimate failure mode being owing to crushing of the UHPC layer at the mid-span section, as illustrated in Fig. 12(g).

6.2. Load-deflection response

The numerically obtained load–deflection plots for the seven specimens are compared with the experimentally obtained ones in Fig. 13. The two curves (numerical and experimental) for each beam are close to each other, and the predicted peak loads also match very well with the experimental ones. The experimental and FE yield and ultimate loads are listed in Table 3, and the experimental and FE load–deflection characteristics are presented in Table 4. The errors in the prediction of yield and ultimate loads are, respectively, 4% − 18% and 1% − 9%. Yet, the errors in the prediction of deflection at yield load, ulti-

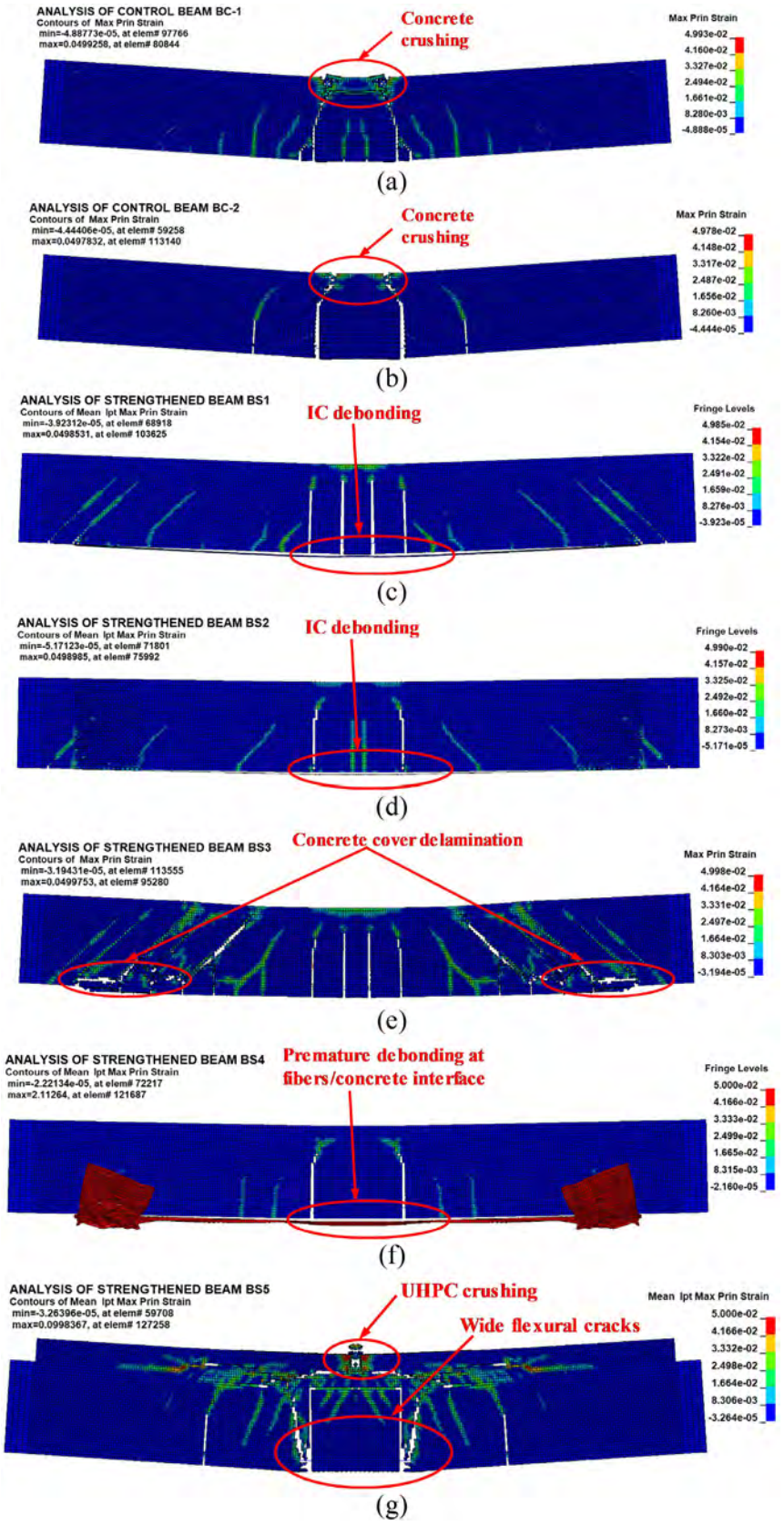

Fig. 12. FE failure modes for beams: (a) BC-1; (b) BC-2; (c) BS1; (d) BS2; (e) BS3; (f) BS4; (g) BS5.

mate deflection, deflection ductility, energy ductility, and energy dissipation at the ultimate state are 5% − 21%, 0% − 10%, 1% − 20%, 6% − 16%, and 1% − 16%, respectively. As identified from Fig. 13 and Table 4, the numerically predicted effective stiffness of the test specimens compares well with the test results with error varying from 3% to 21%. Fig. 13 evidently illustrates that the FE models simulated the

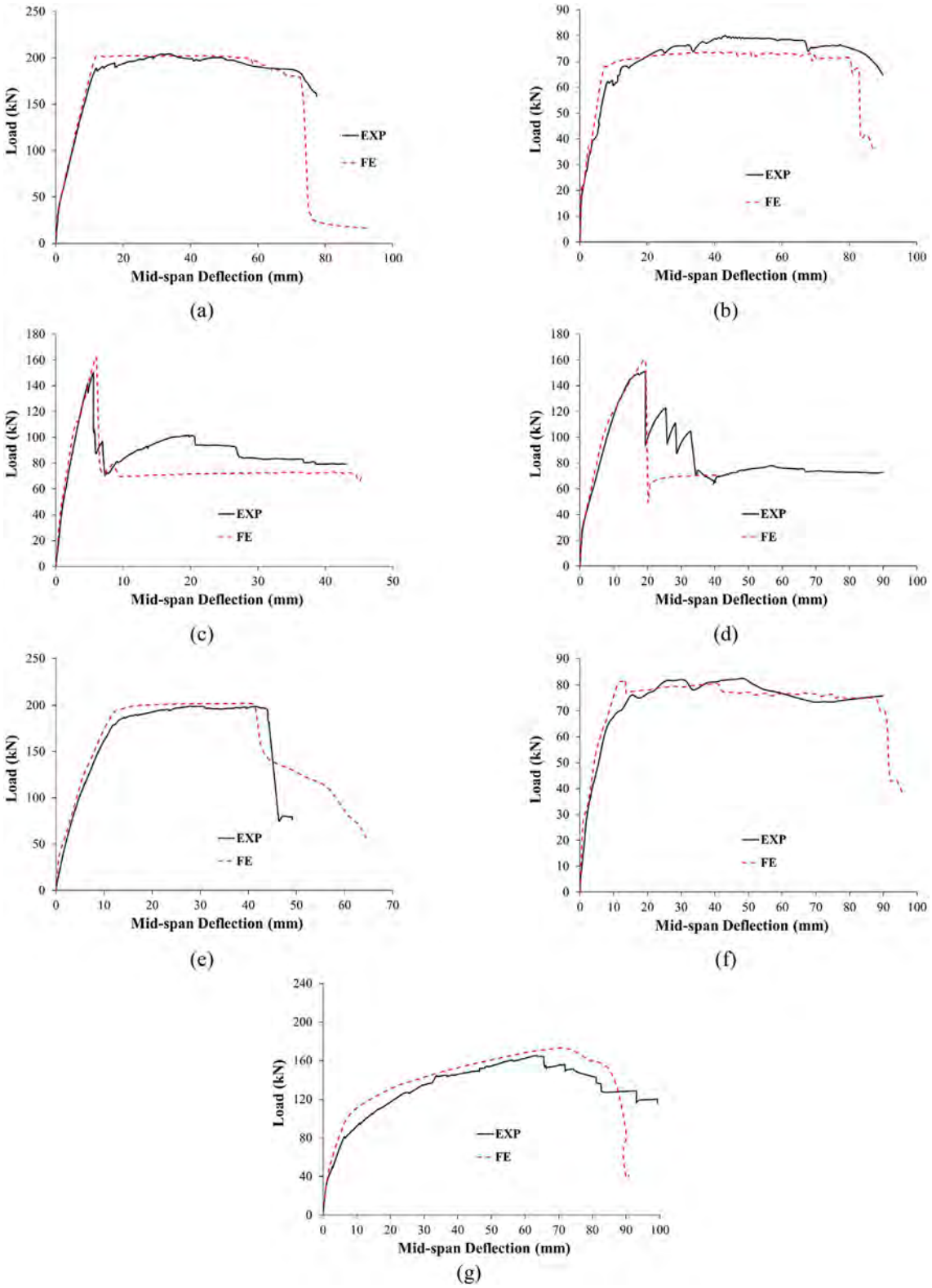

Fig. 13. Load-deflection comparison for beams: (a) BC-1; (b) BC-2; (c) BS1; (d) BS2; (e) BS3; (f) BS4; (g) BS5.

softening behavior very effectively, which verifies the precision of the constitutive and contact models used in this work. The FE modeling confirmed the good performance of the innovative hybrid strengthening technique owing to its ductile behavior. It also verified the good behavior of the NSM strengthening system for beam BS3; however, it supported its need to have FRP U-anchorage at the ends of NSM steel rebars to inhibit concrete cover delamination. The numerical study showed that both externally bonded steel plate and CFRP sheets could give a considerable improvement in the flexural resistance of RC beams; however, they result in brittle failure modes due to IC debonding. In addition, the FE modeling confirmed the very poor behavior of continuous carbon fiber sheets combined with cementitious matrix in flexural retrofitting of RC beams due to the premature debonding at the fibers-to-concrete interface.

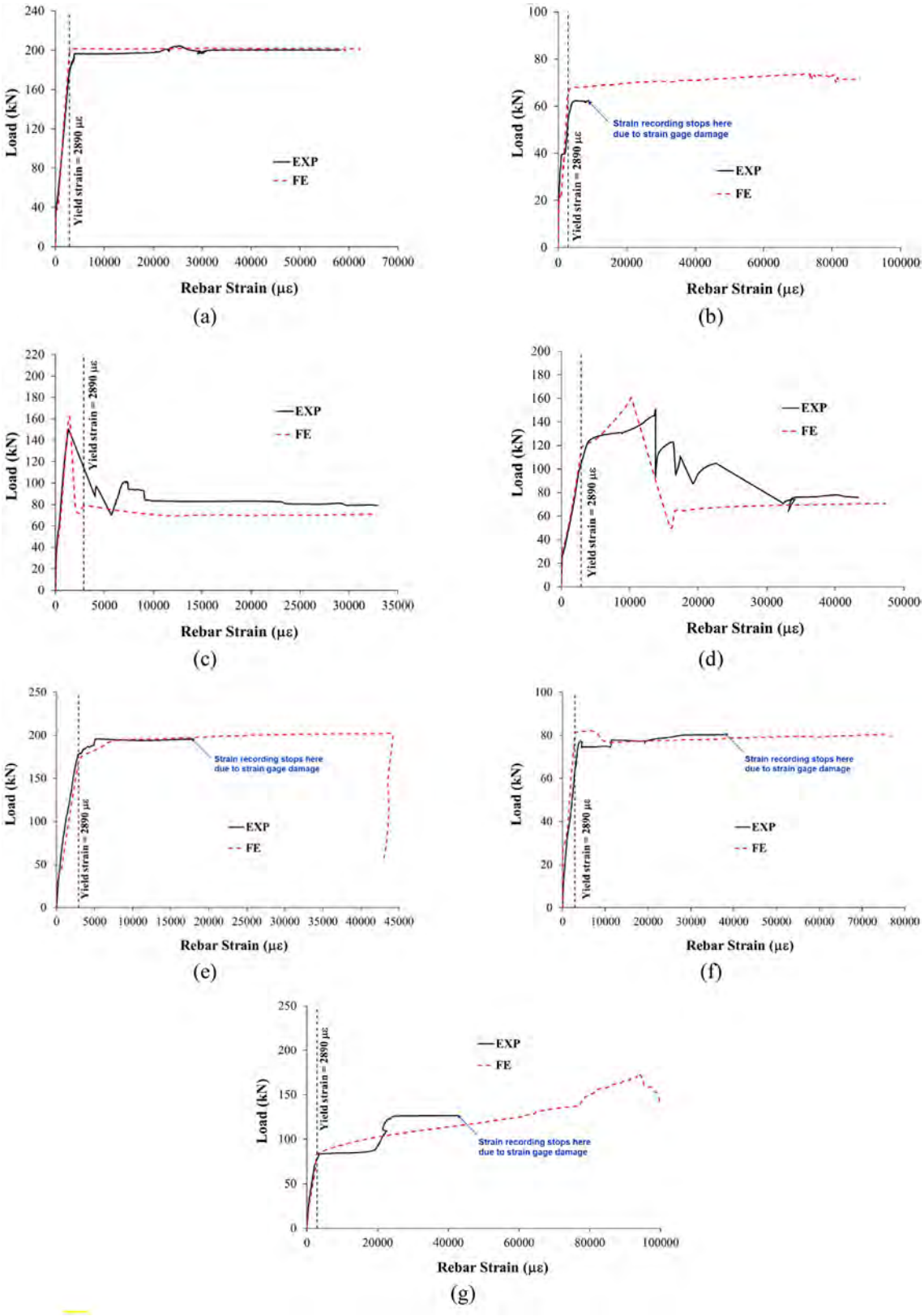

Fig. 14. Comparison plots of measured and FE load vs. strain of bottom rebars at mid-span of beams: (a) BC-1; (b) BC-2; (c) BS1; (d) BS2; (e) BS3; (f) BS4; (g) BS5.

6.3. Strain gage results

Fig. 14 shows comparison plots of measured and numerically predicted load versus strain of main steel rebars at mid-span of tested specimens. Table 4 presents numerical and experimental bottom steel rebar strains at the ultimate state for tested beams. It should be noted that for beams BC-1, BS3, BS4, and BS5, strain gages attached to bottom steel rebars were damaged during the experiments, and their recordings were discontinued, as seen in Fig. 14(b), (e), (f) and (g). It is explicable from Table 4 and Fig. 14 that the FE strains are in good

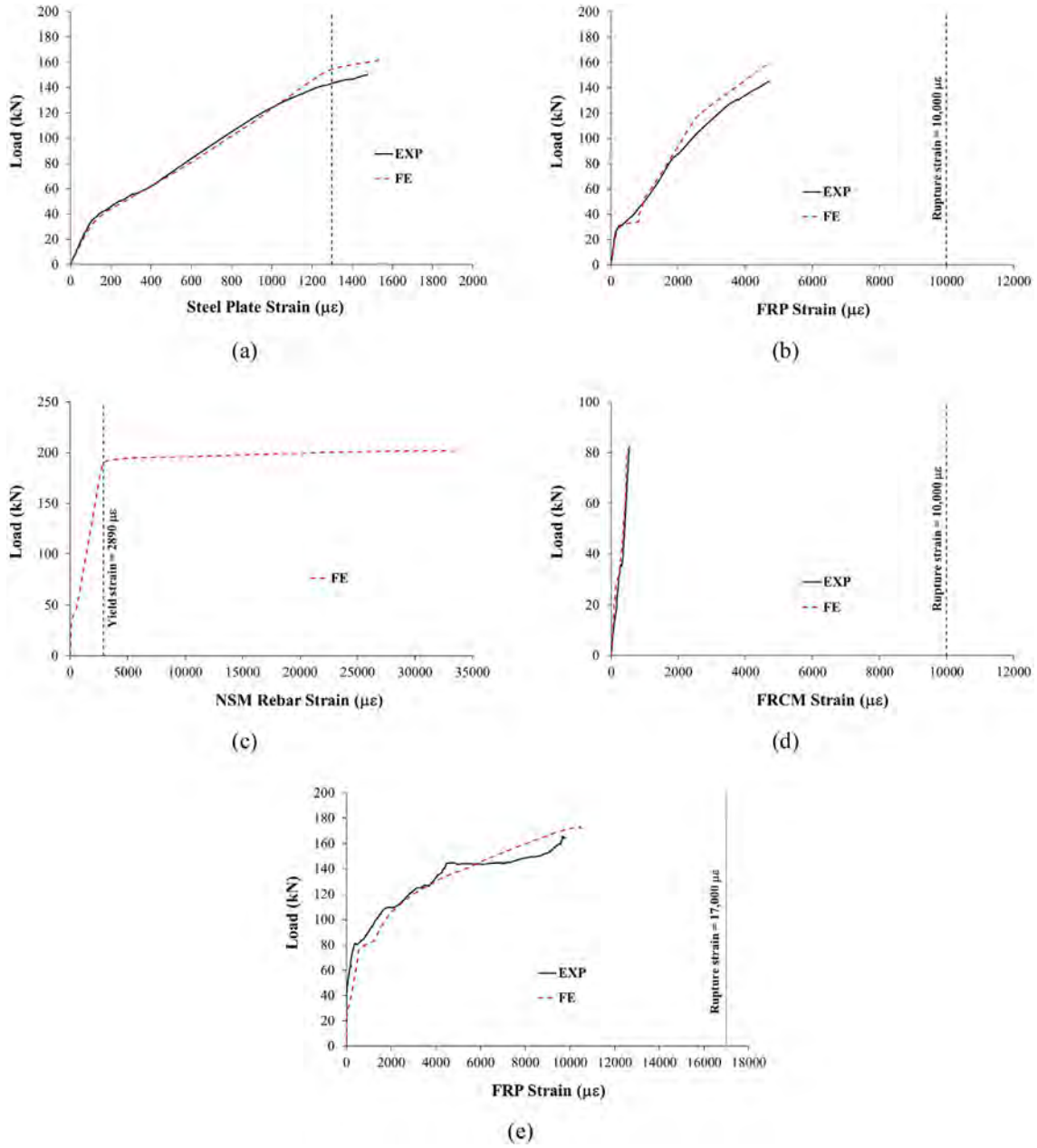

Fig. 15. Comparison plots of measured and FE load vs. strain at mid-span of strengthening system: (a) Steel plate of BS1; (b) CFRP sheets of BS2; (c) NSM steel rebars of BS3; (d) FRCM composite of BS4; (e) NSM CFRP strips of BS5.

conformity with experiments. The large strains recorded (or numerically predicted) for main steel rebars at mid-span of specimens BC-1, BC-2, BS3 and BS5 confirm their ductile behavior at the ultimate state. For beam BS1, yielding was not recorded (or predicted) for main steel rebar up to the ultimate limit state due to the early IC debonding. Even though yielding was noticed for the main steel rebar of beam BS2 before reaching its ultimate state, as seen in Table 4 and Fig. 14(d), strain ductility at ultimate state (ratio of rebar strain at ultimate state to its yield value) was very much less compared to beams BS3 and BS5. Fig. 15 depicts comparison plots of measured and predicted load versus longitudinal strain at mid-span of strengthening system for beams BS1 to BS5. In addition, Table 4 enlists numerical and experimental values of ultimate longitudinal strains at mid-span of strengthening layers for upgraded beams. The numerically predicted values match well with the experimental readings with errors in prediction ranging from 1% to 7%. For beam BS1, yielding was recorded (and predicted) for steel plate, and then the plate debonded from the concrete surface, and its strain decreased. For specimen BS2, CFRP sheets debonded from the concrete surface at a strain of about 4700 με (about 47% of their rupture strain). For beam BS3, strain gages attached to NSM steel rebars were damaged before testing, and their readings were not available. However, as per the FE modeling results, NSM steel rebars experienced large strains at the ultimate state, indicating ductile behavior of the strengthened beam, as seen in Fig. 15(c) and Table 4. For CFRCM-upgraded beam BS4, very low strains of about 550 με were measured (and predicted) at mid-span of carbon fiber sheets due to the premature debonding as discussed previously (see Table 4 and Fig. 15(d)). For specimen BS5 that was upgraded with the innovative hybrid UHPC/NSM system, large strains of about 9800 με and 10,550 με were measured and predicted, respectively, at mid-span of NSM CFRP strips at ultimate state, which were about 58% and 62% of the rupture value, respectively.

Table 6
Details of beams used in the parametric study.

Beam ID	Strengthening scheme
Group 1: Beams strengthened with bonded steel plates	
BS6	Same as BS1 but with t_p = 7 mm and adding side plates at end of flexural strengthening plate (Fig. 16)
BS7	Same as BS1 but with t_p = 10 mm and adding side plates at end of flexural strengthening plate (Fig. 16)
BS8	Same as BS1 but with t_p = 15 mm and adding side plates at end of flexural strengthening plate (Fig. 16)
BS9	Same as BS1 but with t_p = 20 mm and adding side plates at end of flexural strengthening plate (Fig. 16)
Group 2: Beams strengthened with externally bonded CFRP sheets	
BS10	Same as BS2 but with 3 layers of CFRP sheets
BS11	Same as BS2 but with 4 layers of CFRP sheets
BS12	Same as BS2 but with 5 layers of CFRP sheets
BS13	Same as BS2 but with 8 layers of CFRP sheets
Group 3: Beams strengthened with NSM rebars	
BS14	Strengthened with 2ϕ16 mm NSM GFRP rebars
BS15	Same as BS3 but with the addition of CFRP end anchorage (Fig. 19)
BS16	Same as BS14 but with the addition of CFRP end anchorage (Fig. 19)
Group 4: Beams strengthened with FRCM composite	
BS17	Strengthened with 14 layers of FRCM composite (PBO fabric reinforced cementitious matrix)
BS18	Strengthened with 20 layers of FRCM composite (PBO fabric reinforced cementitious matrix)
Group 5: Beams strengthened with hybrid UHPC/NSM system	
BS19	Same as BS5 but with replacing the NSM CFRP strips with 4ϕ13 of NSM CFRP rebars (Fig. 23)
BS20	Same as BS5 but with replacing the NSM CFRP strips with 2ϕ20 of NSM steel rebars (Fig. 23)

7. Parametric study

The calibrated FE models were employed to carry out a parametric study for the five different strengthening systems, as discussed below.

7.1. Steel Plate-strengthened beams

Even though the plate thickness of beam BS1 was designed so that the flexural strength of the specimen would be close to that of the unstrengthened beam BC-1, the measured and predicted flexural capacities of specimen BS1 were about 74% and 80%, respectively, of that for control beam BC-1 as seen in Table 3. This is due to the IC debonding of the plate, which was not considered in the design phase, as discussed previously. Larger plate thicknesses could have been used to increase the beam's flexural strength. Accordingly, another four beams BS6 to BS9 - having a plate thickness of 7 mm to 20 mm - were numerically studied as illustrated in Table 6. As seen before in Fig. 12(c), high shear stresses developed in the shear span of beam BS1 near the end of the plate. With increased plate thickness and hence higher shear force in the shear span, these stresses may cause concrete cover delamination at the end of steel plates, which has to be avoided. Therefore, for beams BS6 to BS9, additional bolted side plates have been added to the strengthening system, as seen in Fig. 16. These side plates were designed to provide more shear strength at the location of plate cutoff points, and they were assumed to be anchored to the beam concrete via four high strength threaded rods, as seen in Fig. 16(a) and (c). Numerically predicted yield and ultimate loads for specimens BS6 to BS9 are shown in Table 7. Also, with the assumption of the perfect bond at the plate-to-concrete interface, yield and ultimate loads for beams BS6 to BS9 were analytically calculated and enlisted in Table 7. Key FE results of load–displacement response are presented in Table 8 for beams BS6 to BS9. Similar to beam BS1, yielding was not numerically predicted for the main steel rebar of beams BS6 to BS9 up to their peak load, and they failed suddenly due to IC debonding, as seen in Fig. 16(d) and Table 8. Numerically predicted load versus mid-span deflection plots for steel plate-upgraded specimens are presented in Fig. 16(e). It is clear that as the plate thickness increases, deflection at the ultimate load decreases, and the behavior became more brittle. Fig. 17 depicts the influence of steel plate thickness on the behavior of retrofitted specimens with respect to flexural strength enhancement, increase in effective stiffness, and steel plate debonding strain. It is explicable from Fig. 17 (a) that as the plate thickness increased from 5 to 15 mm, the enhancement in peak load increased from 119 to 148%; nevertheless, it decreased to 146% when the plate thickness increased to 20 mm. None of the steel-plated beams was able to have flexural capacity gain close to that given by control specimen BC-1. For the economic design of strengthening systems, it is therefore recommended not to use the steel plate strengthening technique to provide flexural strength enhancement exceeding 100%. However, steel plates were successful at increasing the effective beam stiffness by 160 to 455% as the thickness of the steel plate increased from 5 to 20 mm (see in Fig. 17(b)). As identified in Fig. 17(c), the numerically predicted steel plate debonding strain was compared with the debonding strain of the ACI 440.2R-17 [20] given by:

$$\varepsilon_{sd} = 0.41\sqrt{\frac{f'_c}{E_s t_p}}(Units:\ N,\ mm) \tag{3}$$

where f'_c = specified concrete strength; E_s = elastic modulus of steel plates, assumed as 2×10^5 MPa; t_p = thickness of steel plate. It is evident that the ACI equation significantly overestimated the IC debonding strain of all specimens. Thus, in order to provide an accurate estimate of the steel plate debonding strain, the equation of the ACI 440.2R-17 [20] was revised, based on the FE analysis results, as:

$$\varepsilon_{sd} = \frac{0.26\sqrt{f'_c}}{E_s^{0.45} t_p^{0.8}}(Units: N, mm) \tag{4}$$

The IC debonding strain calculated using the proposed Eq. (4) was plotted versus steel plate thickness, as seen in Fig. 17(c) and a good match with the FE results was noticed. Additionally, Eq. (4) was incorporated in the section analysis procedure discussed in Sec. 4 to compute the ultimate load of steel plate-upgraded specimens, and the results are enlisted in Table 7. It is clearly identified that the analytical prediction considering IC debonding at the plate-to-concrete interface provided a good match in comparison with the FE results, with the ratio of FE-to-analytical peak load varying from 0.97 to 1.09 as seen in Table 7.

7.2. CFRP-strengthened beams

Although the CFRP thickness of specimen BS2 was designed so that the peak load of the beam would be close to that of the control specimen BC-1, the measured and predicted peak loads of specimen BS2 were about 74% and 79%, respectively, of that for control beam BC-1 as seen in Table 3. This is due to the IC debonding of the CFRP sheets, which has been measured (and predicted) to occur at a strain of about 4700 με. This value is about 88% of the debonding strain of the ACI 440.2R-17 [20] given by Eq. (3), which has been used to design specimen BS2. Larger CFRP sheet thicknesses could have been used to increase the beam's flexural strength. Accordingly, another four beams BS10 to BS13 having 3 to 8 CFRP layers were numerically investigated, as illustrated in Table 6. It should be noted that similar to beam BS2, CFRP U-wraps were provided at the end of longitudinal CFRP sheets; however, the number of transverse CFRP layers in beams BS10 to BS13 was assumed equal to the number of longitudinal layers. Numerically predicted yield and ultimate loads for specimens BS10 to BS13 are shown in Table 7. In addition, yield and ultimate loads for

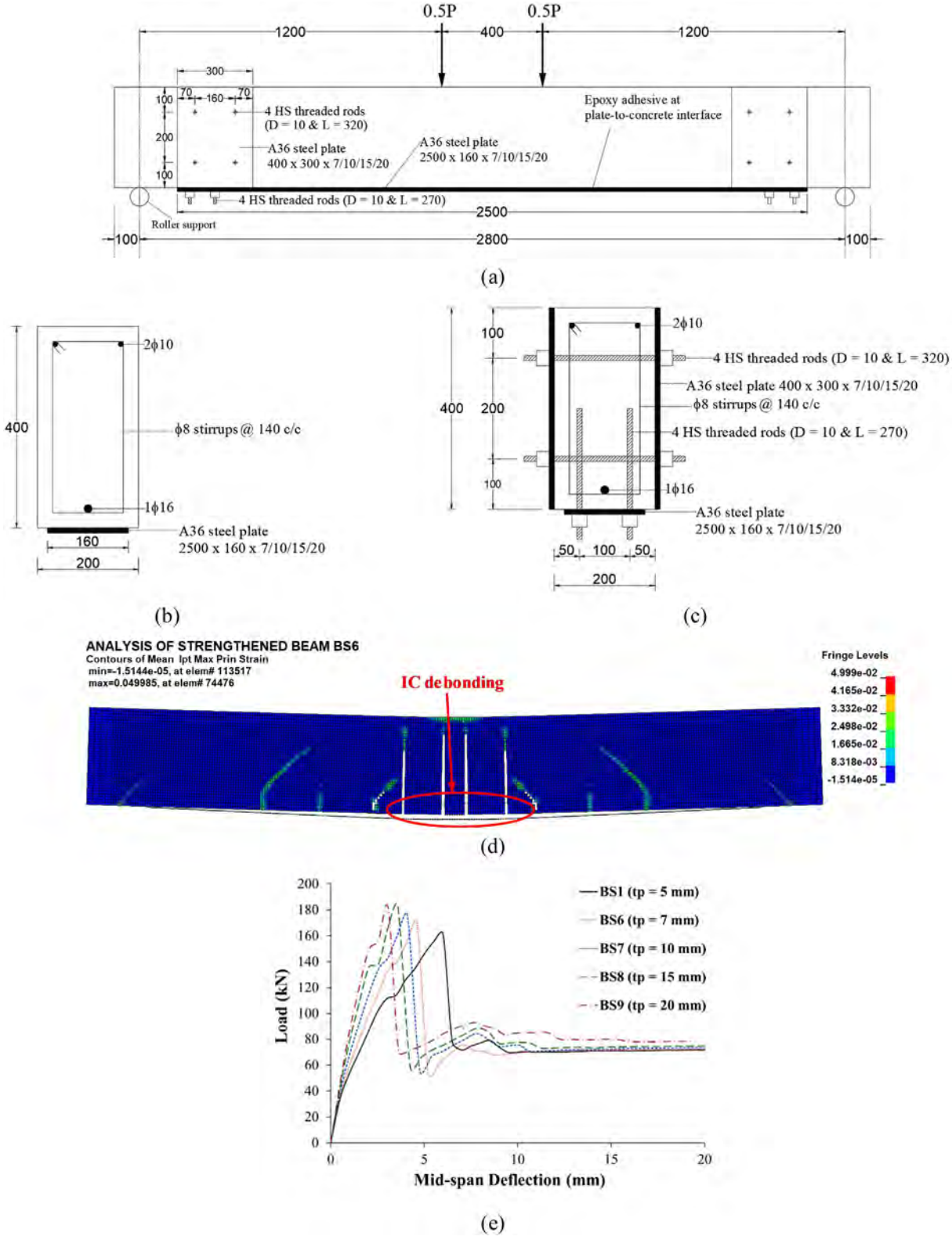

Fig. 16. Details and FE results of steel plate-strengthened beams (Note: All dimensions are in mm): (a) Elevation of BS6 to BS9; (b) Section of BS6 to BS9 at mid-span; (c) Section of BS6 to BS9 at end of steel plate; (d) FE mode of failure of BS6; (e) FE load–deflection curves of beams.

beams BS10 to BS13 were analytically calculated as per Sec. 4 and enlisted in Table 7. Key FE results of load–displacement characteristics are displayed in Table 8 for beams BS10 to BS13. As per the FE results, yielding was predicted for the main steel rebar of all CFRP-strengthened beams except BS13. However, as per the analytical modeling, the yielding of the main steel rebar was only predicted for beams BS10 and BS11. FE load–deflection plots for CFRP-strengthened specimens are presented in Fig. 18(a). It is clear that as the thickness of the CFRP sheet increases, deflection at the ultimate load decreases and the behavior became more brittle. Fig. 18(b) to (d) present effect of FRP

Table 7
Predicted yield and ultimate loads for beams used in the parametric study.*

Beam ID	Yield load (P_y) (kN)			Ultimate load (P_u) (kN)			% Gain in flexural strength	
	FE	AN	FE/AN	FE	AN	FE/AN	FE	AN
Control beams								
BC-1	197	183	1.08	202	184	1.10	175	179
BC-2	62	64	0.97	74	66	1.11	0	0
*Beams strengthened with bonded steel plates***								
BS1	NY	178 (NY)	–	162	189 (149)	0.86 (1.09)	119	186 (125)
BS6	NY	221 (NY)	–	170	235 (174)	0.73 (0.98)	131	255 (163)
BS7	NY	280 (NY)	–	176	298 (177)	0.59 (0.99)	138	350 (167)
BS8	NY	379 (NY)	–	183	392 (182)	0.47 (1.00)	148	492 (175)
BS9	NY	NY (NY)	–	181	460 (186)	0.39 (0.97)	146	595 (181)
Beams strengthened with externally bonded CFRP sheets								
BS2	117	131	0.90	160	170	0.94	118	157
BS10	159	164	0.97	169	192	0.88	129	189
BS11	162	197	0.82	176	209	0.84	139	216
BS12	172	NY	–	178	224	0.79	141	238
BS13	NY	NY	–	176	250	0.70	139	277
Beams strengthened with NSM rebars								
BS3	171	192	0.89	202	194	1.04	174	193
BS14	98	97	1.01	191	180	1.06	160	172
BS15	176	192	0.92	205	194	1.06	179	193
BS16	97	97	1.01	193	180	1.07	162	172
Beams strengthened with FRCM composite								
BS17	149	134	1.12	192	172	1.11	160	160
BS18	189	164	1.15	194	191	1.01	163	189
Beams strengthened with hybrid UHPC/NSM system								
BS5	83	91	0.92	173	167	1.03	135	153
BS19	88	92	0.96	172	172	1.00	133	160
BS20	90	94	0.95	175	167	1.05	137	152

* EXP = experimental; FE = finite element; AN = analytical.
** Values within brackets are for analytical modeling considering debonding at plate/concrete interface.

Table 8
FE results for beams used in the parametric study*

Beam ID	Δ_y (mm)	Δ_u (mm)	K_s (kN/m)	E_u (kN.m)	μ_Δ	μ_E	ε_{su} (με)**	$\varepsilon_{stm,u}$ (με)**	Failure mode
Control beams									
BC-1	11.4	73.2	17,302	13.75	6.4	5.8	***62,234***	–	SY-CC
BC-2	6.2	83.0	10,032	5.82	13.5	13.1	***88,092***	–	SY-CC
Beams strengthened with bonded steel plates									
BS1	NY	6.2	26,117	0.61	–	–	1460	***1541***	DB-CC
BS6	NY	4.6	37,005	0.53	–	–	1090	1119	DB-CC
BS7	NY	4.3	40,925	0.51	–	–	824	856	DB-CC
BS8	NY	3.8	48,370	0.47	–	–	928	632	DB-CC
BS9	NY	3.3	55,655	0.40	–	–	707	481	DB-CC
Beams strengthened with externally bonded CFRP sheets									
BS2	9.3	19.5	12,639	2.04	2.1	2.3	***15,877***	4741	SY-DB-CC
BS10	10.3	18.0	15,408	2.27	1.7	1.7	***30,323***	3666	SY-DB-CC
BS11	9.5	15.6	17,097	1.95	1.6	1.5	***22,450***	2865	SY-DB-CC
BS12	9.2	13.6	18,651	1.75	1.5	1.4	***15,573***	2293	SY-DB-CC
BS13	NY	9.3	22,925	1.36	–	–	2768	1603	DB-CC
Beams strengthened with NSM rebars									
BS3	9.7	42.4	17,600	7.50	4.4	4.2	***44,217***	***33,358***	SY-DL-CC
BS14	7.4	47.0	13,219	7.14	6.3	7.9	***40,204***	13,150	SY-DL-CC
BS15	8.8	65.8	19,980	12.42	7.5	7.4	***66,480***	***55,474***	SY-CC
BS16	7.5	51.3	13,034	7.97	6.9	8.8	***52,144***	14,260	SY-FR-CC
Beams strengthened with FRCM composite									
BS17	9.4	15.1	15,865	1.87	1.6	1.5	***11,774***	5288	SY-DB-CC
BS18	11.3	11.9	16,753	1.50	1.1	1.1	***5797***	3715	SY-DB-CC
Beams strengthened with hybrid UHPC/NSM system									
BS5	5.0	86.7	16,614	12.46	17.3	20.2	***99,710***	10,558	SY-CC
BS19	4.2	100.6	21,127	14.97	24.1	29.6	***120,270***	8513	SY-CC
BS20	4.2	112.4	21,385	17.40	26.7	33.5	***129,160***	***16,295***	SY-CC

*Δ_y = mid-span deflection at yielding of main steel; Δ_u = mid-span deflection at ultimate state; K_s = effective pre-yield stiffness; E_u = energy dissipated at ultimate state; μ_Δ = deflection ductility ratio = Δ_u/Δ_y; μ_E = energy ductility as calculated from Eq. (1); ε_{su} = ultimate strain of main tension steel rebars at mid-span; $\varepsilon_{stm,u}$ = ultimate strain of strengthening material at mid-span; SY-CC = steel yielding followed by concrete crushing at mid-span; DB-CC = intermediate crack debonding followed by concrete crushing at mid-span; SY-DB-CC = steel yielding at mid-span followed by intermediate crack debonding and finally concrete crushing at mid-span; SY-DL-CC = steel yielding at mid-span followed by concrete cover delamination at end of NSM rebars and finally concrete crushing at mid-span; SY-FR-CC = steel yielding at mid-span followed by fracture of FRP rebar and finally concrete crushing at mid-span; NY = No steel yielding.
**Values in italic bold font indicate steel yielding.

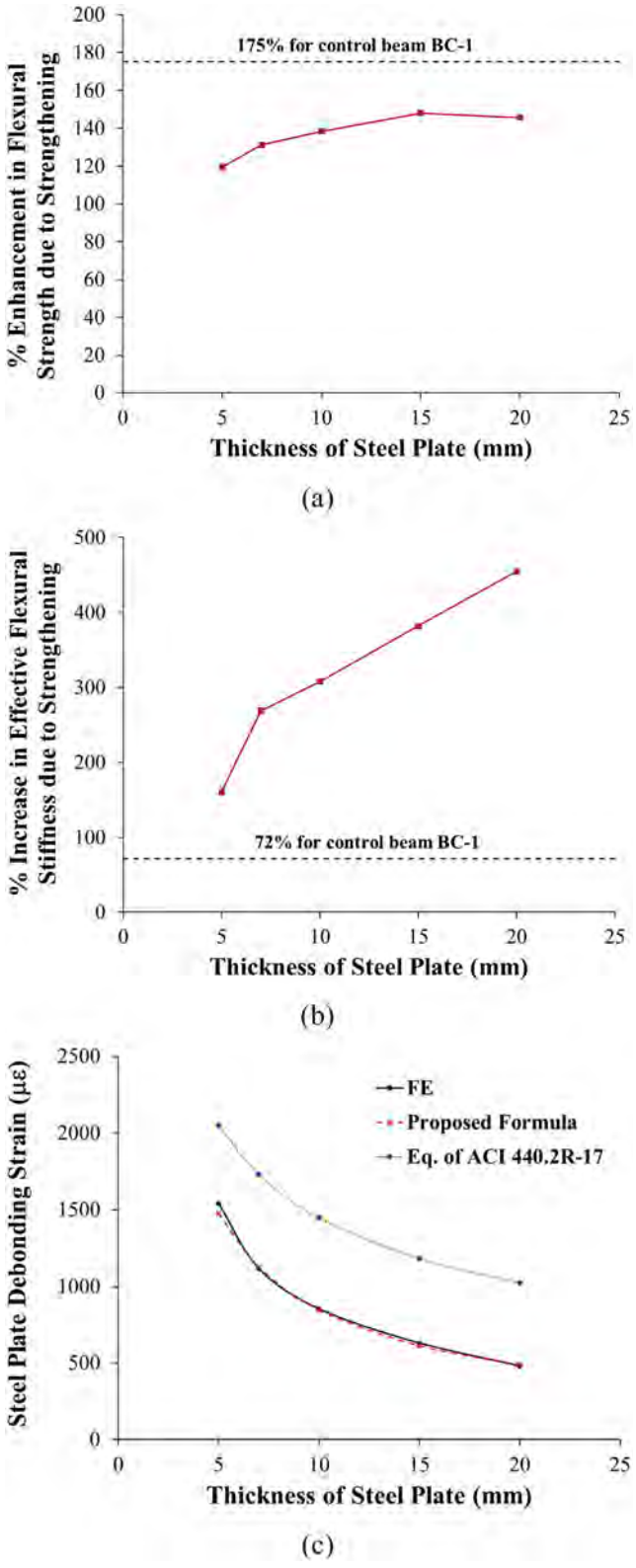

Fig. 17. Effect of steel plate thickness on behavior of strengthened beams (based on FE analysis).

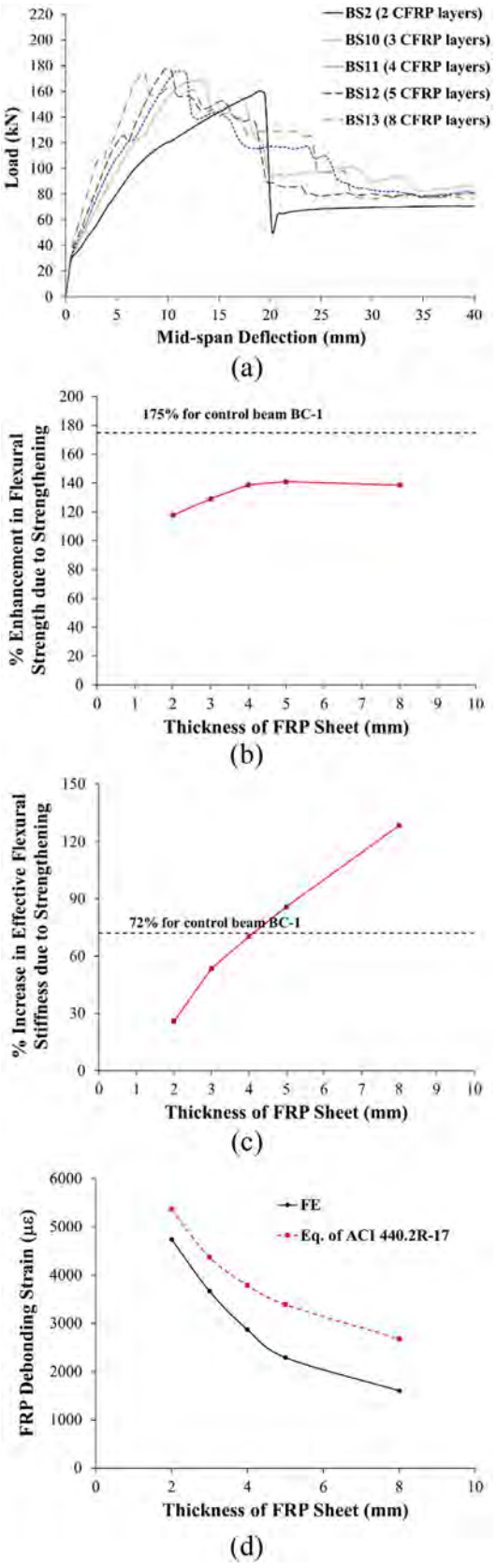

Fig. 18. Effect of FRP thickness on behavior of FRP-strengthened beams (based on FE analysis).

thickness on the behavior of strengthened beams with respect to flexural strength enhancement, increase in effective stiffness, and CFRP debonding strain. It is explicable from Fig. 18(b) that as the FRP thickness increased from 2 to 5 mm, the enhancement in peak load increased from 118 to 141%; yet it decreased to 139% when the FRP thickness increased to 8 mm. None of the CFRP-upgraded beams was able to have flexural capacity gain close to that given by the

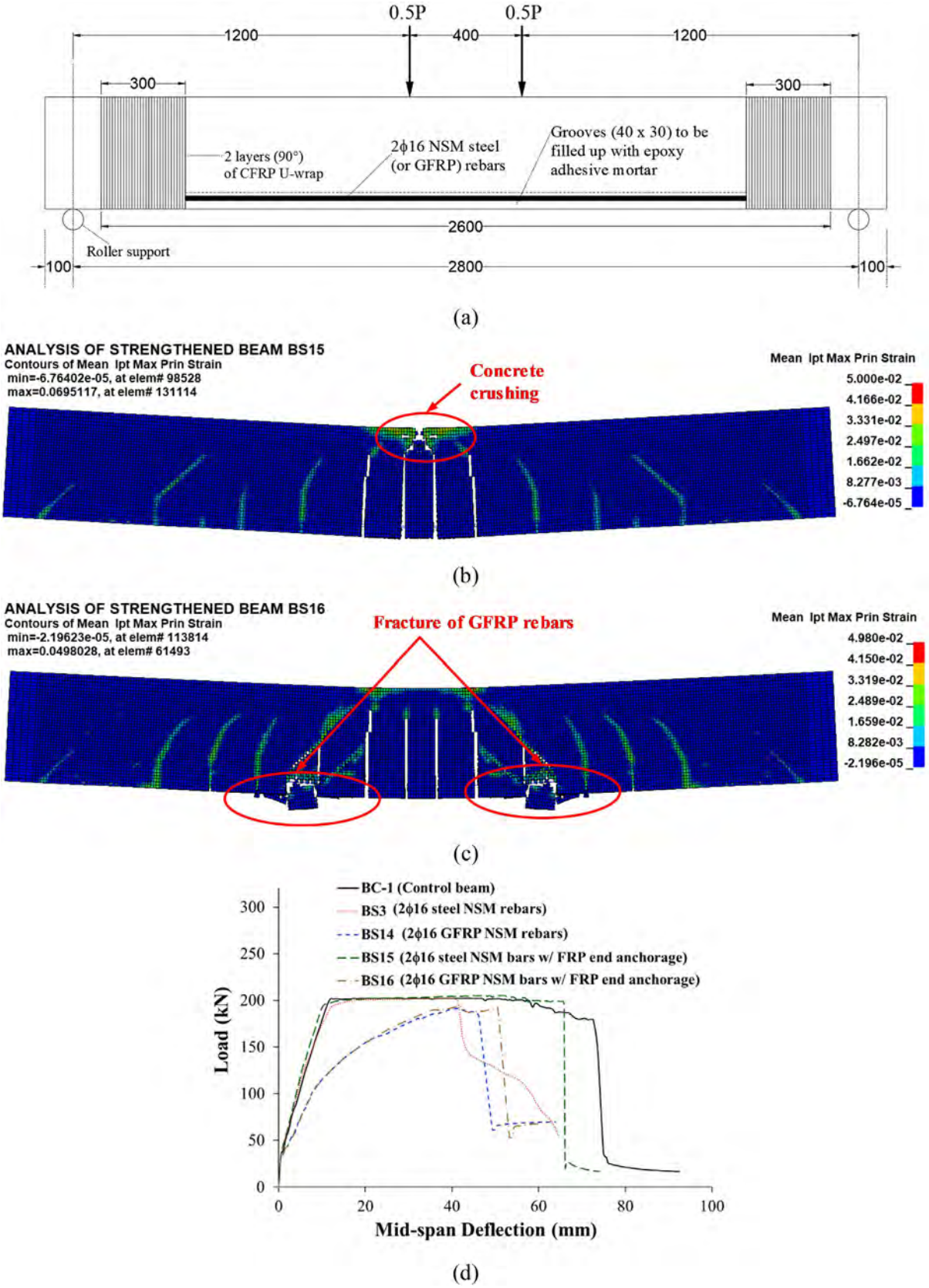

Fig. 19. Details and FE results of NSM rebar-strengthened beams (Note: All dimensions are in mm): (a) Elevation of BS15 and BS16; (b) FE mode of failure of BS15; (c) FE mode of failure of BS16; (d) FE load–deflection curves of beams.

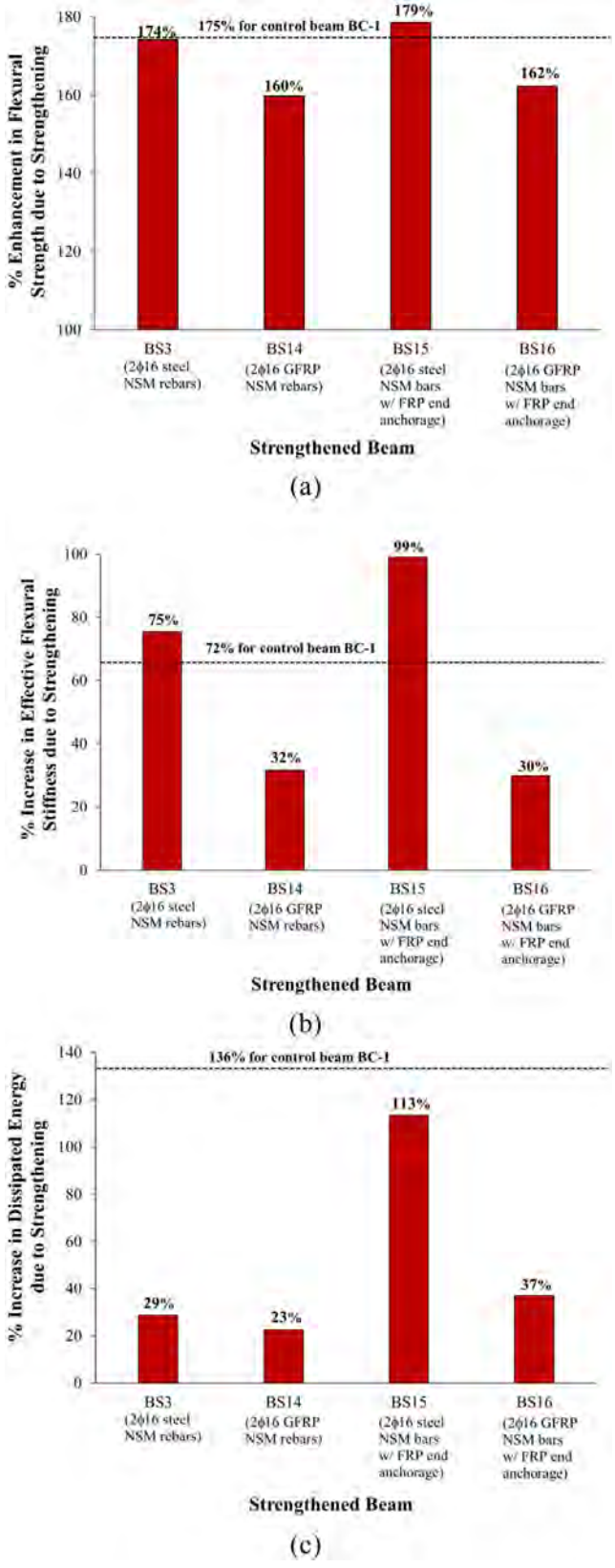

Fig. 20. Behavior comparison of NSM rebar-strengthened beams (based on FE analysis).

control specimen BC-1. Therefore, it is not recommended to use externally bonded CFRP sheets to provide flexural capacity enhancement exceeding 100%. As seen in Fig. 18(c), CFRP sheets increased the effective beam stiffness by 26 to 129% as the FRP thickness increased from 2 to 8. As identified in Fig. 18(d), the numerically predicted FRP debonding strain was compared with the debonding strain of the ACI 440.2R-17 [20] given by Eq. (3). Even though it is a design equation and should give a conservative assessment, it is evidenced from Fig. 18(d) that the ACI equation overestimated the IC debonding strain of all specimens, and the overestimation increases as the number of CFRP layers increases. This conclusion was also confirmed by previous studies in the literature [28,45]. Elsanadedy et al. [28] collected the available experimental data on FRP-upgraded RC beams and one-way slabs that failed in flexure due to IC debonding. The database comprised of 203 specimens. The IC debonding strain of the specimens was compared with available models in codes and researchers. It was depicted that among five models of different codes considered in the study, the ACI model was the most non-conservative, where it overestimated the debonding strain for 62.6% of the data (127 specimens). In another study, Elsanadedy et al. [45] tested FRP-strengthened RC one-way slabs, which failed in flexure by IC debonding. The ACI model was found to overestimate the analytical prediction of the peak load of tested slabs by up to 12%.

7.3. NSM Rebar-strengthened beams

For beam BS3 upgraded with NSM steel rebars, a parametric study was carried out to evaluate the impact of the type of NSM rebars and provision of FRP U-anchorage at the ends of NSM rebars on the performance of strengthening system. In this regard, beams BS14 to BS16 were numerically investigated, as seen in Table 6. Beam BS14 was the same as BS3 except with the replacement of 2ϕ16 NSM steel rebars with 2ϕ16 NSM GFRP rebars. Properties of ϕ16 GFRP rebars used in the FE modeling are listed in Table 2, and they were selected to provide flexural capacity that is very close to beam BS3. As pointed out previously, both experimental and FE results for beam BS3 supported the need to have FRP U-anchorage at the ends of NSM steel rebars to inhibit concrete cover delamination. Therefore, specimens BS14 and BS15 were, respectively, designed to be the same as beams BS3 and BS14 except that they were provided with two layers of CFRP U-wrap at the ends of NSM rebars as illustrated in Fig. 19(a). In addition to FE analysis, the analytical prediction was conducted as per Sec. 4 to compute the yield and ultimate loads of specimen BS15. However, for specimens BS14 and BS16, the yield and ultimate section capacities were estimated as per both ACI 318-19 [30] and ACI 440.1R-15 guidelines [46]. Both numerically and analytically predicted yield and ultimate loads for specimens BS14 to BS16 are shown in Table 7. In addition, key FE results of load–displacement characteristics are displayed in Table 8 for beams BS14 to BS16. The FE failure mode for strengthened beam BS14 was similar to BS3, and it was because of the separation of concrete cover at the termination point of NSM GFRP rebars. However, for strengthened beams BS14 and BS15, the FRP U-wraps were successful at mitigating the concrete cover separation, and the failure mode of specimen BS15 was very much similar to the control beam BC-1 (concrete crushing in the top side after the formation of flexural cracks) as seen in Fig. 19(b). Yet, failure of specimen BS16 was initiated by the formation of flexural cracks, and then GFRP rebars fractured near mid-span, causing spalling of parts of concrete cover as depicted from Fig. 19(c). FE load–deflection plots for beams strengthened with NSM rebars are shown in Fig. 19(d). It is clear from the curves that the post-cracking stiffness of beams with GFRP rebars are considerably less than that of beams with NSM steel rebars. It is also explicable that the load–deflection curve of BS15 is very much similar to that of unstrengthened beam BC-1. Fig. 20 presents a comparison of the behavior of specimens upgraded with NSM rebars in terms of flexural strength enhancement (with respect to control specimen BC-2), increase in effective stiffness, as well as the increase in dissipated energy. Fig. 20 identifies that the use of FRP U-anchorage enhanced the response parameters, especially the energy dissipation.

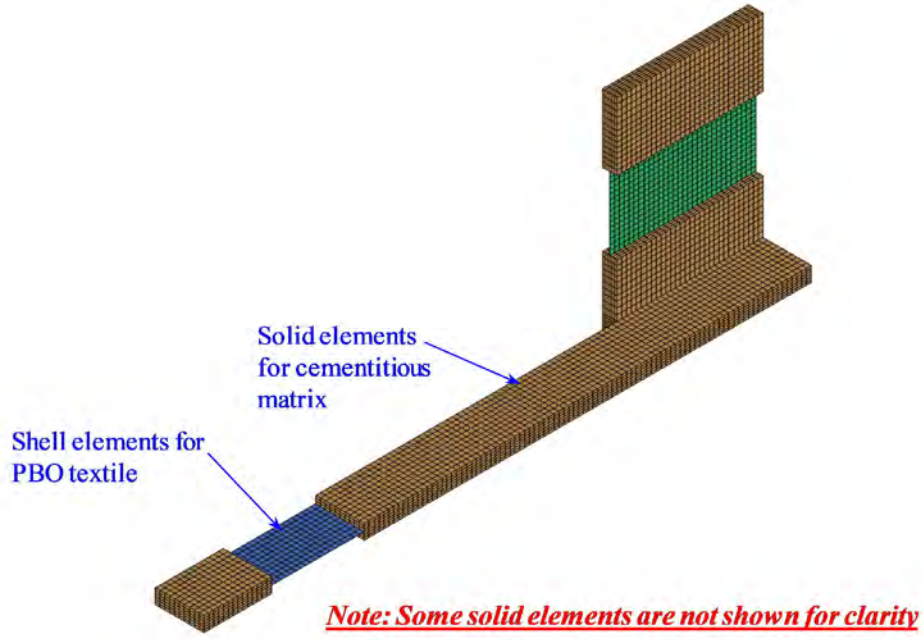

(a)

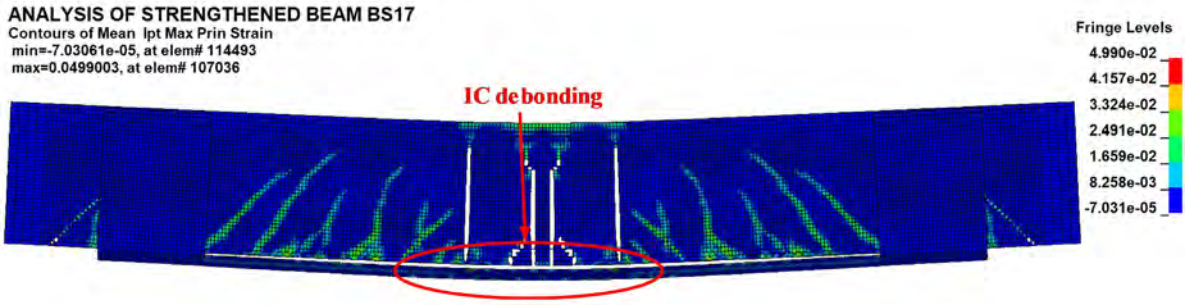

(b)

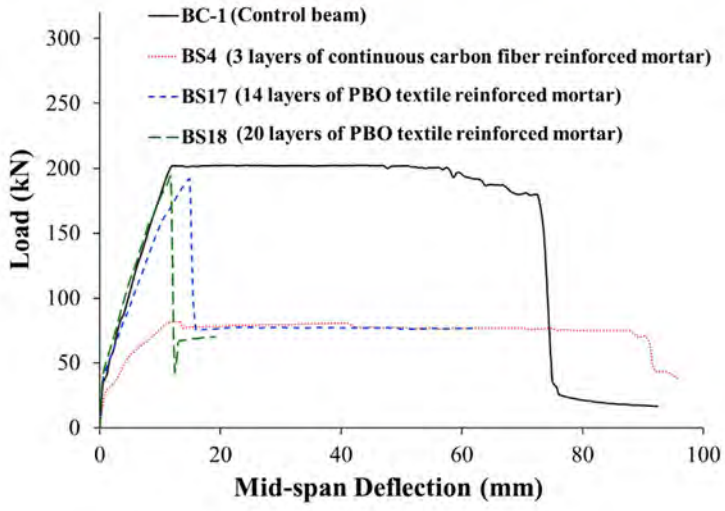

(c)

Fig. 21. Details and FE results of FRCM-strengthened beams: (a) FE mesh of one-quarter of FRCM layers for BS17; (b) FE mode of failure of BS17; (c) FE load–deflection curves of beams.

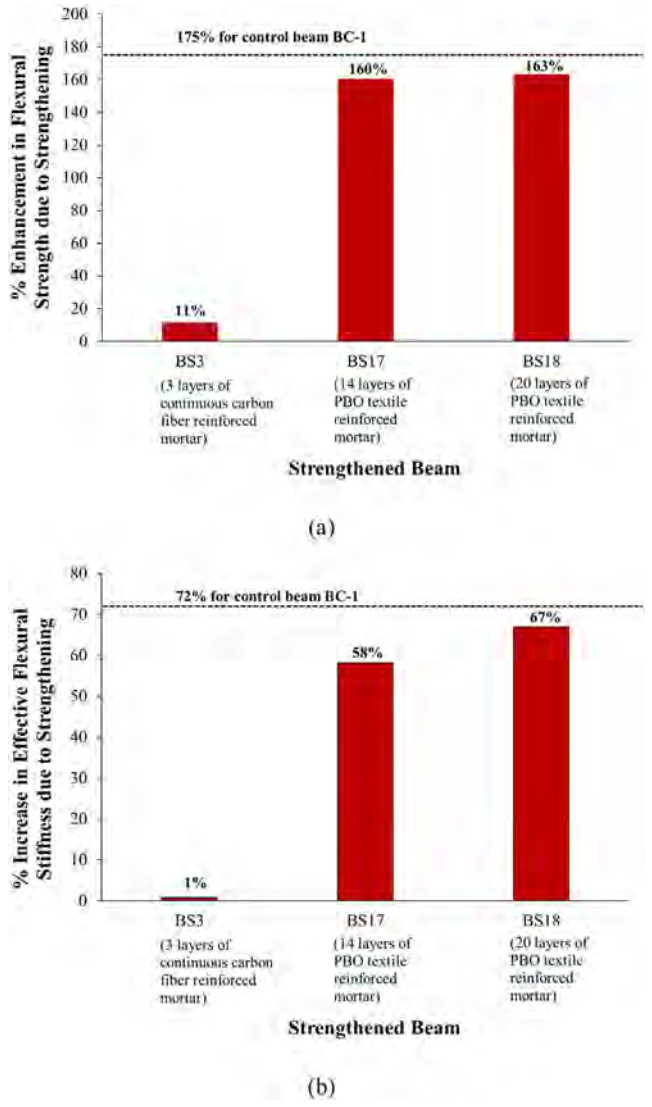

Fig. 22. Behavior comparison of FRCM-strengthened beams (based on FE analysis).

It is clear from the figure that the behavior of beams with NSM steel rebars was generally better than those with NSM GFRP rebars. The best performance was given by specimen BS15 for which the flexural strength enhancement was a little more than that of control beam BC-1 and the increase in energy dissipation was about 83% of that of BC-1. However, the increase in effective stiffness of BS15 was about 38% more than that provided by BC-1 due to the use of epoxy adhesive and repair mortar to fill the grooves of NSM rebars.

7.4. FRCM-strengthened beams

As discussed previously, in beam BS4, the cementitious mortar was not able to impregnate the continuous carbon fiber sheets, which resulted in poor fiber–matrix interaction. As mentioned in the literature [1,9], better fiber–matrix interfaces could be attained if continuous fiber sheets are substituted by textiles. Consequently, two more beams BS17 and BS18 were numerically studied. These beams were strengthened with PBO (Polybenzoxazole) textile impregnated with polymer-modified cementitious mortar to form textile reinforced mortar (TRM) composite – also called FRCM composite. Properties of PBO textile and cementitious mortar are provided in Table 2. As depicted from Table 6, in beam BS17, 14 TRM layers were designed to provide approximately the same strength and stiffness of two layers of CFRP (or CFRCM) composite, and hence its performance can be compared with BS2 and BS4. In beam BS18, 20 layers of TRM composite were used for flexural strength enhancement to have the same strength and stiffness of three layers of CFRP sheets. This beam was numerically studied in order to investigate the impact of the number of TRM layers on the performance of TRM-retrofitted specimens and to compare its behavior with CFRP-upgraded beam BS10. In the FE modeling of BS17 and BS18, the mortar was incorporated. As seen in Fig. 21(a), eight-node brick elements were utilized to simulate the mortar volume. However, PBO textile was smeared into an equivalent continuous sheet using the equivalent layer thickness provided in Table 2, and it was hence represented using 4-node shell elements of Belytschko-Tsay formulation [40] as illustrated in Fig. 21(a). A perfect bond was input between the mortar and textile elements. Whereas, tiebreak contact was input at the mortar-to-concrete interface with formulas for tensile and shear bond strengths as given in Table 5. It should be noted that these formulas were calibrated in another study [9]. It should also be noted that similar to specimen BS4, 14 and 20 layers of TRM U-wrap were, respectively, used as end anchorage of specimens BS17 and BS18 (Fig. 21(a)).

Numerically predicted yield and ultimate loads for specimens BS17 to BS18 are shown in Table 7. Ignoring the mortar contribution, yield and ultimate loads for beams BS17 and BS18 were analytically calculated (see Table 7) as per the procedure outlined in Sec. 4 for CFRP-strengthened beams. Key FE results of load–deflection parameters are displayed in Table 8 for beams BS17 and BS18. It is noted that in comparison with the FE results, the analytical models underestimated the peak load of TRM-upgraded beams by 1%–11% (see Table7). This may be attributed to ignoring the mortar contribution in section analysis calculations. This also may reveal the relevance of the ACI 440.2R-17 model in assessing the flexural capacity of TRM-strengthened sections. As predicted from the FE modeling, failure of specimens BS17 and BS18 was close to that of CFRP-retrofitted specimens. It was due to IC debonding at the mortar-to-concrete interface, which initiated at the bottom end of large flexural cracks in the maximum-moment zone, and then it propagated to the beam ends (see Fig. 21(b)). FE load–deflection plots for CFRCM-strengthened beams are presented in Fig. 21(c). It is clear that as the thickness of TRM composite increases, deflection at the ultimate load decreases, and the behavior became more brittle. Fig. 22(a) and (b) present the effect of type and number of fabric layers on the behavior of specimens with regard to both flexural strength enhancement and increase in effective stiffness. It is explicable from Fig. 22(a) that as the type of fabric changed from continuous fiber sheets to open mesh textile, the performance dramatically improved, and both flexural strength and effective stiffness enhancements increased significantly from 11% to 160% and 1% to 58%, respectively. However, increasing the number of TRM layers from 14 to 20 has almost no impact on the peak load increase, and little influence on the effective stiffness increase (see Fig. 22).

7.5. Beams strengthened with hybrid UHPC/NSM system

In the innovative strengthening technique, the type of NSM strengthening system was numerically investigated. As seen in Table 6, two beams BS19 and BS20 were numerically studied. In beams BS19 and BS20, the NSM CFRP strips in beam BS5 were, respectively, replaced with 4ϕ13 mm CFRP rebars and 2ϕ20 mm steel rebars, as seen in Fig. 23(a) and (b). Properties of ϕ13 CFRP and ϕ20 steel rebars are given in Table 2, and they were designed to provide almost the same flexural capacity as beam BS5. In addition to FE analysis, the

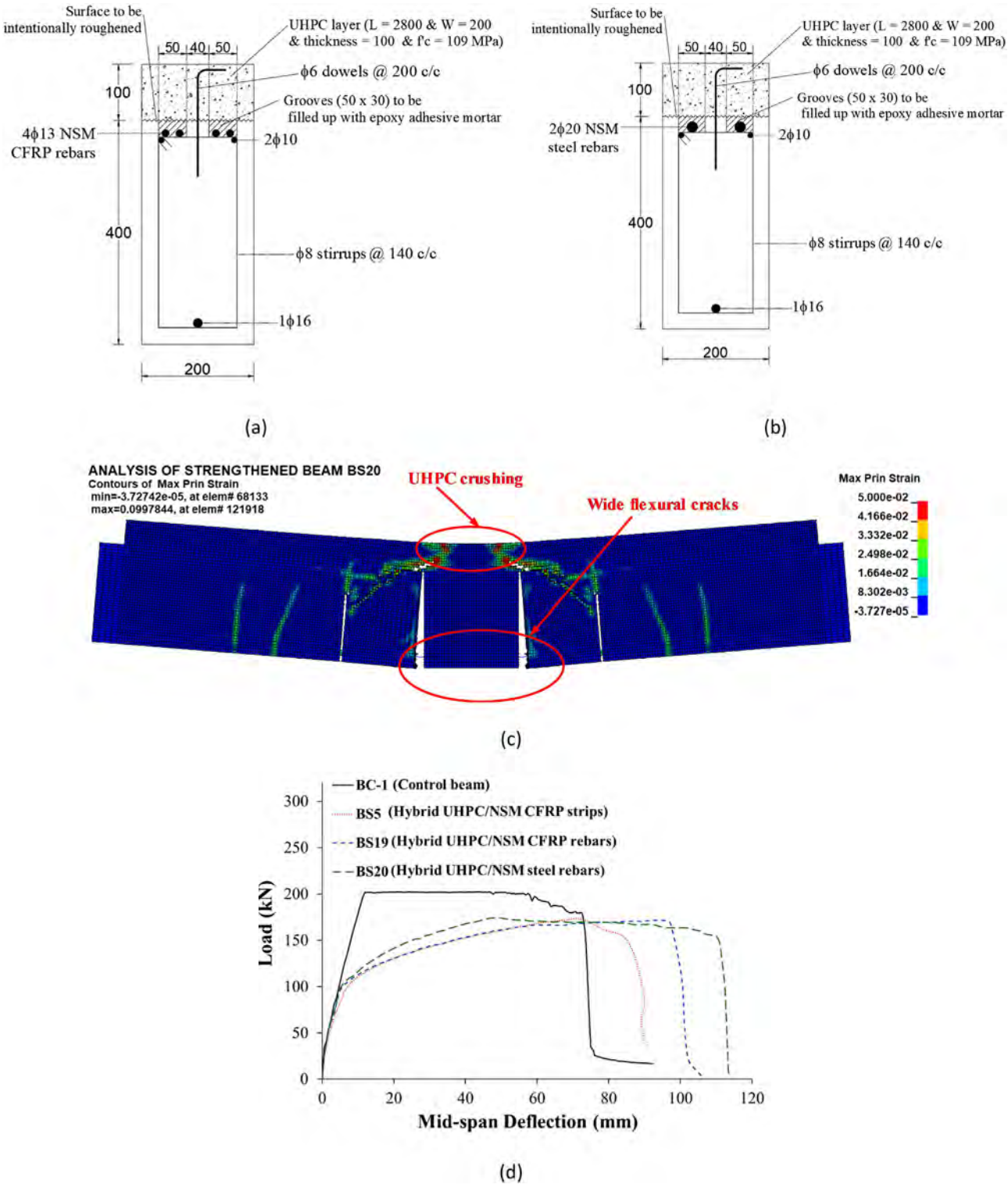

Fig. 23. Details and FE results of beams strengthened with hybrid UHPC/NSM system (Note: All dimensions are in mm): (a) Mid-span section of BS19; (b) Mid-span section of BS20; (c) FE mode of failure of BS20; (d) FE load–deflection curves of beams.

yield and ultimate section capacities were estimated as per both ACI 318–19 [30] and ACI 440.1R-15 guidelines [46]. Both numerically and analytically predicted yield and ultimate loads for specimens BS19 and BS20 are shown in Table 7. In addition, key FE results of load–deflection characteristics are displayed in Table 8 for beams BS19 and BS20. The FE failure modes for strengthened beams BS19 and BS20 were similar to specimen BS5. It was because of large flexural cracking in the constant-moment zone, which propagated upwards till the UHPC layer, with the ultimate failure mode being due to crushing of the UHPC layer, as illustrated in Fig. 23(c) for spec-

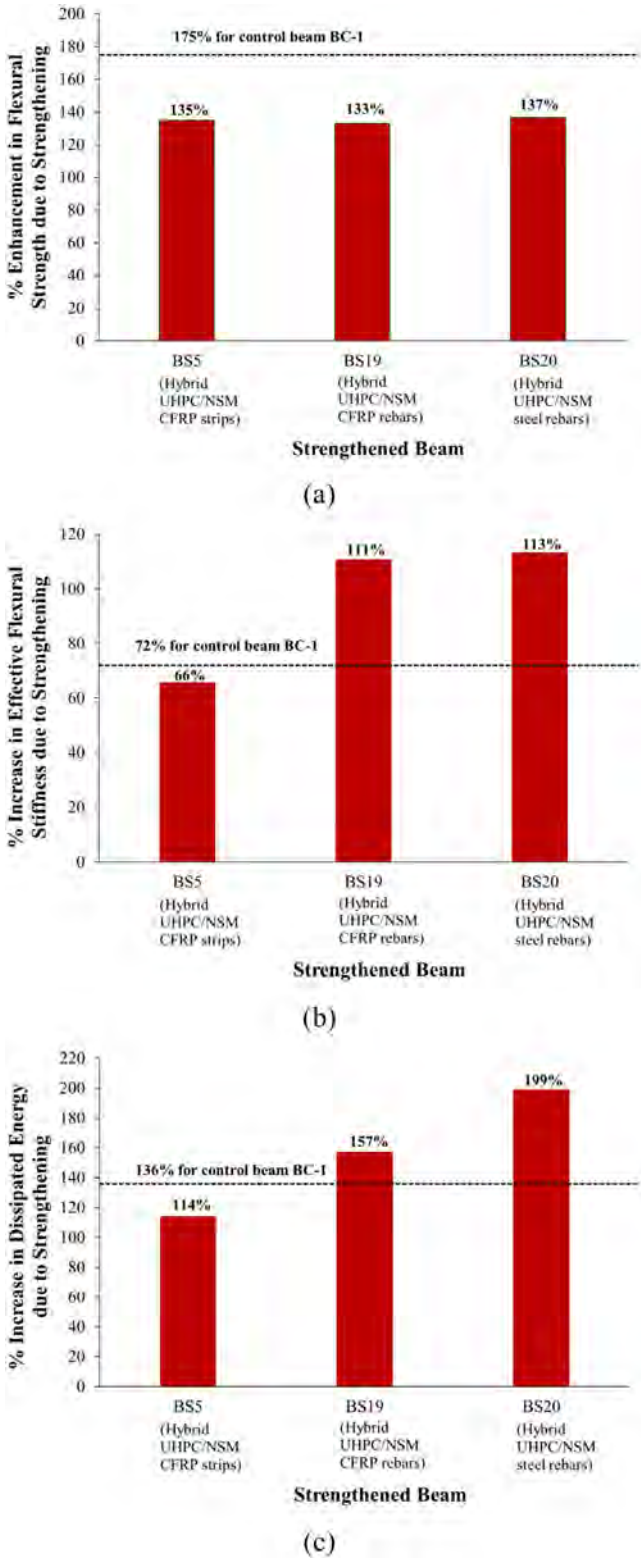

Fig. 24. Behavior comparison of beams strengthened with hybrid UHPC/NSM system (based on FE analysis).

imen BS20. Numerically predicted load–deflection plots for specimens upgraded with hybrid UHPC/NSM system are shown in Fig. 23(d). It is clear from the curves that all three specimens have almost the same behavior with beam BS20, having the largest ultimate deflection. Fig. 24 presents a comparison of the behavior of specimens retrofitted with hybrid UHPC/NSM system in terms of flexural strength enhancement, increase in effective stiffness, as well as increase in dissipated energy. Fig. 24(a) identifies that all three strengthened beams gave approximately the same flexural strength enhancement; however, the behavior of BS19 and BS20 is better than BS5 in terms of effective stiffness enhancement (Fig. 24(b)). Concerning the energy dissipation, the best performance was provided by specimen BS20 for which the increase in dissipated energy was significantly more than beams BS5 and BS19. In conclusion, it is recommended to use NSM steel rebars instead of CFRP strips or CFRP rebars in the innovative system. It is also not recommended to use this system for flexural strength enhancement exceeding 100%.

7.6. Comparison of strengthening techniques

In order to compare the five different investigated flexural strengthening techniques, the behavior of strengthened beams, which have been initially designed to give almost the same peak load as control specimen BC-1, was compared in terms of numerically predicted load–deflection characteristics. For the 20 numerically studied beams enlisted in Tables 7 and 8, the comparison could be then carried out between beams: BS1 (from Group 1), BS2 (from Group 2), BS3, BS14, BS15, BS16 (from Group 3), BS4, BS17 (from Group 4), BS5, BS19 and BS20 (from Group 5). However, in this section, the comparison was conducted between the best beam of each strengthening technique. Thus, the performance of beams BS1, BS2, BS15, BS17, and BS20 was compared, as seen in Fig. 25. The load–deflection curves of the five beams versus the control specimen BC-1 were plotted in Fig. 25(a). With regard to the load–deflection curve, the best performance was provided by beam BS15 and BS20. Fig. 25(b) displays a comparison of both FE and analytical prediction of the peak load of upgraded beams with control specimen BC-1, as well as a comparison between analytically and numerically predicted ultimate loads. It is noted from Fig. 25(b) that as per the basis of the design of different strengthening systems, the analytically predicted ultimate load of strengthened beams became in close agreement with that of control beam BC-1 with the ratio ranged from 0.90 to 1.05. In comparison with control specimen BC-1, beam BS15 with steel NSM rebars had almost the same ultimate capacity; yet peak capacity for other strengthening techniques ranged from 79% to 95% of that of beam BC-1. Fig. 25(c) to (f), respectively, show a comparison of different strengthening systems in terms of effective stiffness ratio, ultimate deflection, energy dissipated, and deflection ductility ratio. In these figures, the response of each strengthening system was compared with control specimen BC-1. Based on the four response parameters, the innovative hybrid UHPC/NSM system was the best ductile strengthening technique followed by NSM steel rebars, and all other strengthening systems had brittle behavior due to the IC debonding at strengthening layer-to-concrete interface. In conclusion, in flexural upgrading of RC beams, it is recommended to use either NSM steel rebars or hybrid UHPC/NSM system. However, the flexural strength enhancement of the latter may be limited due to the less effective depth of the added NSM reinforcement.

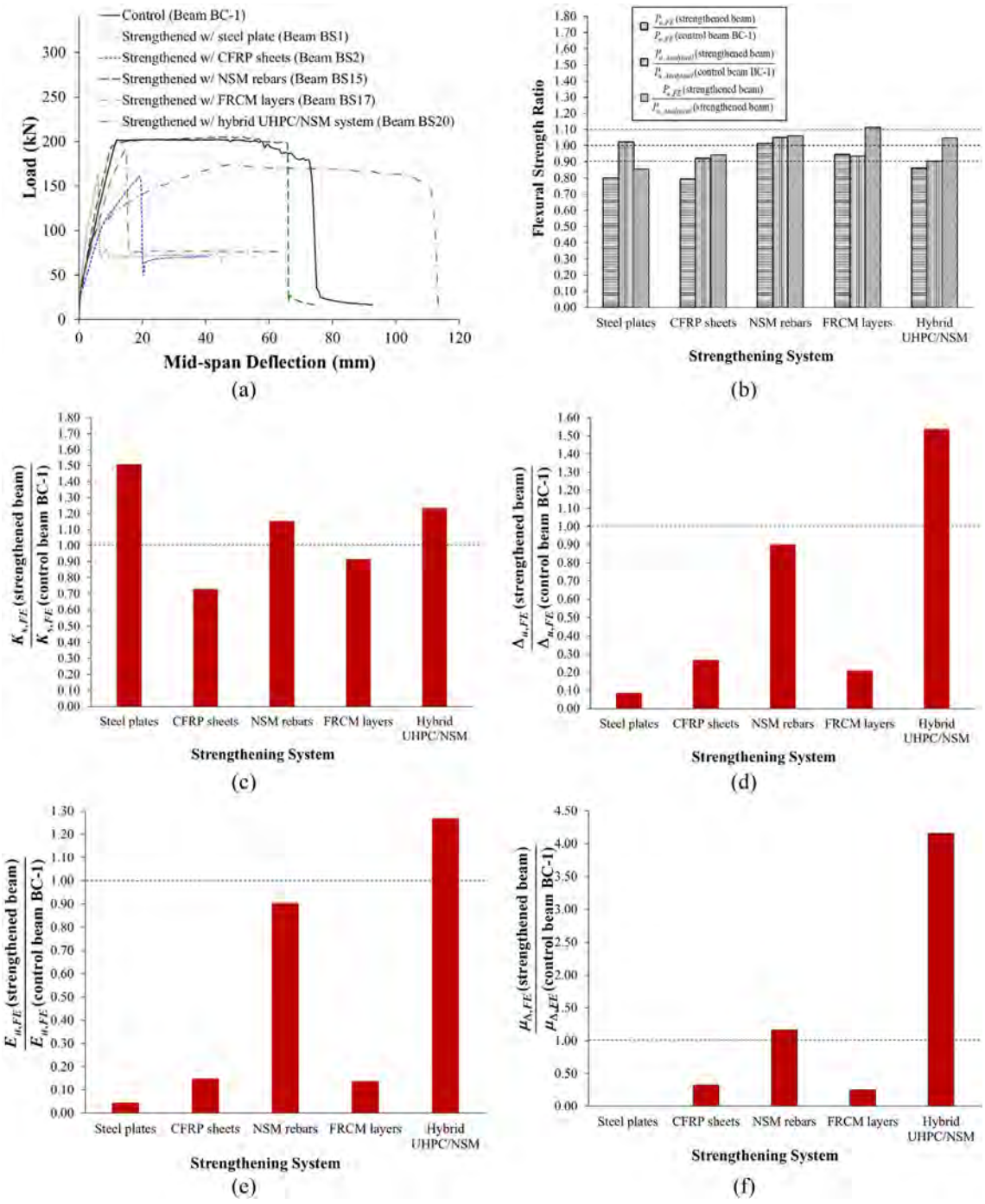

Fig. 25. Behavior comparison of beams strengthened with different systems (based on FE analysis).

8. Conclusions

The key outcomes of this research can be outlined as follows:

1. For the steel plate upgrading system, it was found that IC debonding at the plate-to-concrete interface is the dominant failure mode. As the plate thickness increases, post-cracking effective stiffness increases while mid-span deflection at peak load decreases, and the behavior turns out to be more brittle. The analytical modeling with the assumption of the perfect bond at the plate-to-concrete interface significantly overestimated the flexural capacity. For accurate analytical prediction, debonding has to be considered once the steel plate strain exceeds a certain limit and in this regard, proposed Eq. (4) may be used to assess the plate debonding strain. It is worth noting that this formula may be revised upon the availability of more experimental data. For the economic design of strengthening systems, it is not suggested to use bonded steel plates for flexural capacity enhancement exceeding 100%.
2. For flexural upgrading of RC beams using externally bonded CFRP sheets, IC debonding at CFRP/concrete interface was the only noticed mode of failure. It is identified that as the thickness of CFRP sheet increases, mid-span deflection at peak load decreases,

and the behavior became more brittle. The model of the ACI 440.2R-17 overestimated the FRP debonding strain. It is not recommended to use externally bonded CFRP sheets to provide flexural capacity enhancement exceeding 100%.

3. In flexural upgrading of beams using NSM rebars, it is recommended to check the shear capacity at the cutoff points of the NSM rebars as per the requirements of the ACI 318-19 code and provide external shear strengthening at those locations if needed (e.g., FRP U-wraps). It is also suggested to use steel rather than GFRP as NSM rebars because the behavior of beams with NSM steel rebars was generally better than those with NSM GFRP rebars.
4. In case of the upgrading of RC beams via externally attached FRCM composites, it is not recommended to utilize continuous fiber sheets with cementitious matrix due to the disability of the matrix to impregnate the fibers and hence the lack of the composite action. This may lead to premature debonding at the fiber/matrix interface and, therefore, a very poor load–deflection response.
5. An innovative hybrid/NSM system was suggested in this study for the flexural upgrading of RC beams. In this technique, it is recommended to use NSM steel rebars rather than CFRP strips or CFRP rebars. It should be noted that in case of suggesting this technique for flexural upgrading of RC beams, crack width at the level of original steel reinforcement has to be controlled at service load levels. The flexural strength enhancement provided by this system is not suggested to exceed 100%. This may be due to the less effective depth of the added NSM reinforcement.
6. In the comparison of the different strengthening systems with respect to failure mode and load–deflection characteristics, it is recommended to use either NSM steel rebars (with FRP U-wraps as end anchorage) or hybrid UHPC/NSM steel rebars as the flexural strengthening of RC beams. This may be attributed to their ductile behavior. However, all other strengthening systems had brittle behavior due to the IC debonding at strengthening layer-to-concrete interface.

9. Data Availability

The raw/processed data required to reproduce these findings cannot be shared at this time due to technical or time limitations.

CRediT authorship contribution statement

Hussein M. Elsanadedy: Conceptualization, Methodology, Writing - original draft. **Husain Abbas:** Visualization, Writing - review & editing. **Tarek H. Almusallam:** Validation, Writing - review & editing. **Yousef A. Al-Salloum:** Supervision, Project administration, Funding acquisition.

Declaration of Competing Interest

The authors declare that they have no known competing financial interests or personal relationships that could have appeared to influence the work reported in this paper.

Acknowledgements

The authors extend their appreciation to the Deputyship for Research & Innovation, “Ministry of Education” in Saudi Arabia for funding this research work through the project number IFKSUHI-140.

References

[1] Elsanadedy HM, Abbas H, Almusallam TH, Al-Salloum YA. Organic versus inorganic matrix composites for bond-critical strengthening applications of RC structures –State-of-the-art review. Compos Part B: Eng, 2019;106947.
[2] Saiidi M, Vrontinos S, Douglas B. Model for the response of reinforced concrete beams strengthened by concrete overlays. ACI Struct J 1990;87(6):687–95.
[3] Júlio ENBS, Branco FAB. Reinforced concrete jacketing - Interface influence on cyclic loading response. ACI Struct J 2008;105(4):471–7.
[4] Aykac S, Kalkan I, Asce AM, Aykac B, Karahan S, Kayar S. Strengthening and repair of reinforced concrete beams using external steel plates. J Struct Eng 2013;139:929–39.
[5] Almusallam TH, Elsanadedy HM, Al-Salloum YA, Alsayed SH. Experimental and numerical investigation for the flexural strengthening of RC beams using near-surface mounted steel or GFRP bars. Constr Build Mater 2013;40:145–61.
[6] Mosallam A, Elsanadedy HM, Almusallam TH, Al-Salloum YA, Alsayed SH. Structural evaluation of reinforced concrete beams strengthened with innovative bolted/bonded advanced FRP composites sandwich panels. Compos Struct 2015;124:421–40.
[7] Almusallam T, Al-Salloum Y, Elsanadedy H, Alshenawy A, Iqbal R. Behavior of FRP-strengthened RC beams with large rectangular web openings in flexure zones: Experimental and numerical study. Int J Concr Struct M 2018;12(1):47.
[8] Almusallam TH, Elsanadedy HM, Al-Salloum YA. Effect of longitudinal steel ratio on behavior of RC beams strengthened with FRP composites – Experimental and FE study. *ASCE*. J Compos Constr 2014;19(1).
[9] Elsanadedy HM, Almusallam TH, Alsayed SH, Al-Salloum YA. Flexural strengthening of RC beams using textile reinforced mortar – Experimental and numerical study. Compos Struct 2013;97:40–55.
[10] Jung K, Hong K, Han S, Park J, Kim J. Prediction of flexural capacity of RC beams strengthened in flexure with FRP fabric and cementitious matrix. Int J Polym Sci 2015;2015:11, Article ID 868541.
[11] Toutanji H, Deng Y. Comparison between organic and inorganic matrices for RC beams strengthened with carbon fiber sheets. ASCE J Compos Constr 2007;11(5):507–13.
[12] Raoof SM, Koutas LN, Bournas DA. Textile-reinforced mortar (TRM) versus fibre-reinforced polymers (FRP) in flexural strengthening of RC beams. Constr Build Mater 2017;151:279–91.
[13] Capozucca R, Magagnini E, Vecchietti MV. Experimental static and dynamic response of RC beams damaged and strengthened with NSM GFRP rod. Compos Struct 2020;241:112100.
[14] Feng R, Liu Y, Zhu J-H, Xing F. Flexural behaviour of C-FRCM strengthened corroded RC continuous beams. Compos Struct 2020;245:112200.
[15] Sezen H. Effectiveness of repair and strengthening methods for reinforced concrete columns and beam-column joints. In: Structures Congress, Vol. 10. Chicago, IL; 2012. p. 2015–24.
[16] Bournas D, Triantafillou T. Strengthening of reinforced concrete columns with near-surface-mounted FRP or stainless steel. ACI Struct J 2009;106(4):495–505.
[17] Jung WT, Park JS, Kang JY, Keum MS. Flexural behavior of concrete beam strengthened by near-surface mounted CFRP reinforcement using equivalent section model. Adv Mater Sci Eng 2017:16, Article ID 9180624.
[18] fib bulletin 14. Externally bonded FRP reinforcement for RC structures. Technical Report prepared by the Working Party EBR of Task Group 9.3, International Federation for Structural Concrete, Lausanne, Switzerland, 2001.
[19] Papanicolaou CG, Triantafillou TC, Papathanasiou M, Karlos K. Textile reinforced mortar (TRM) versus FRP as strengthening material of URM walls: out-of-plane cyclic loading. Mater Struct 2008;41(1):143–57.
[20] ACI Committee 440. Guide for the design and construction of externally bonded FRP systems for strengthening concrete structures. ACI 440.2R-17, American Concrete Institute, Farmington Hills, MI; 2017.
[21] Teng JG, Smith ST, Yao J, Chen JF. Intermediate crack-induced debonding in RC beams and slabs. Constr Build Mater 2003;17(6–7):447–62.
[22] Smith ST, Teng JG. FRP-strengthened RC beams. I: Review of debonding strength models. Eng Struct 2002;24(4):385–95.
[23] Pham H, Al-Mahaidi R. Assessment of available predictions models for the strength of FRP retrofitted RC beams. Compos Struct 2004;66(1–4):601–10.
[24] Fu B, Teng JG, Chen JF, Chen GM, Guo YC. Concrete cover separation in FRP-plated RC beams: mitigation using FRP U-jackets. ASCE J Compos Constr 2017;21(2):04016077.
[25] Al-Saawani MA, El-Sayed AK, Al-Negheimish AI. Assessment of plate-end debonding design provisions for RC beams strengthened with FRP. Lat Am J Solids Struct 2020;17(2).
[26] Zhang D, Shi H, Ueda T, Jin W. Effect of U-shaped anchorages on concrete cover separation in carbon fiber-reinforced polymer-strengthened beams with notches at the sheet end. Struct Concr 2020. https://doi.org/10.1002/suco.201900388.
[27] Bizindavyi L, Neale KW. Transfer lengths and bond strengths for composites bonded to concrete. ASCE J Compos Constr 1999;3(4):153–60.
[28] Elsanadedy HM, Abbas H, Al-Salloum YA, Almusallam TH. Prediction of intermediate crack debonding strain of externally bonded FRP laminates in RC beams and one-way slabs. ASCE J Compos Constr 2014;18(5):04014008.
[29] Al-Atta B, Kalfat R, Al-Mahaidi R, Al-Mosawe A. Mitigation of IC debonding in FRP-plated concrete slabs using patch anchors. Eng Struct 2020;214:110626.
[30] ACI Committee 318. Building code requirements for structural concrete and commentary. ACI 318-19, American Concrete Institute, Detroit, MI, USA; 2019.
[31] ASTM. Standard test method for compressive strength of cylindrical concrete specimens. ASTM C39/C39M - 17, American Society for Testing and Materials, West Conshohocken, PA, USA; 2017.
[32] ASTM. Standard test method for compressive strength of hydraulic cement mortars (using 2-in. or [50-mm] cube specimens). ASTM C109/C109M, American Society for Testing and Materials, West Conshohocken, PA; 2008.
[33] ASTM. Standard test methods for tension testing of metallic materials. ASTM E8/E8M - 16a, American Society for Testing and Materials, West Conshohocken, PA, USA; 2016.

[34] ASTM. Standard test methods and definitions for mechanical testing of steel products. ASTM A370 - 17, American Society for Testing and Materials, West Conshohocken, PA, USA; 2017.
[35] ASTM. Standard test method for tensile properties of polymer matrix composite materials. ASTM D3039/D3039M – 14, American Society for Testing and Materials, West Conshohocken, PA, USA; 2014.
[36] NZS 4203: 1992. New Zealand Standard, Code of practice for general structural design and design loadings for buildings 1; 1992.
[37] Emadi J, Hashemi SH. Flexural study of high strength RC beams strengthened with CFRP plates. World Acad Sci Eng Technol 2011;78:380–4.
[38] Ascionea L, Carozzi FG, D'Antino T, Poggi C. New Italian guidelines for design of externally bonded Fabric-Reinforced Cementitious Matrix (FRCM) systems for repair and strengthening of masonry and concrete structures. Struct Integrity Proc Elsevier; 2018.
[39] Livermore Software Technology Corporation (LSTC). LS-DYNA keyword user's manual, LS-DYNA R11, LSTC, Livermore, CA;, 2018.
[40] Belytschko TB, Tsay CS. Explicit algorithms for non-linear dynamics of shells. J Appl Mech, Appl Mech Div ASME 1981;48:209–31.
[41] Murray YD, Abu-Odeh A, Bligh R. Evaluation of concrete material model 159. Report No. FHWA-HRT-05-063, US Department of Transportation, Federal Highway Administration National Transportation Systems Center, USA; 2007.
[42] Chang FK, Chang KY. A progressive damage model for laminated composites containing stress concentration. J Compos Mater 1987;21:834–55.
[43] Silfwerbrand JL. Failure, distress and repair of concrete structures. In: Delatte N, editor. Failure, Distress and Repair of Concrete Structures. Boca Rotan, FL: CRC Press; 2009.
[44] Ombres L. Analysis of the bond between fabric reinforced cementitious mortar (FRCM) strengthening systems and concrete. Compos Part B-Eng 2015;69:418–26.
[45] Elsanadedy HM, Almusallam TH, Alsayed SH, Al-salloum YA. Experimental and FE study on RC one-way slabs upgraded with FRP composites. KSCE J Civ Eng 2015;19(4):1024–40.
[46] ACI Committee 440. Guide for the design and construction of structural concrete reinforced with FRP bars. ACI 440.1R-15, American Concrete Institute, Detroit, MI, USA; 2015.